Electrical Characterization of Bulk and Thin Film Zinc Oxide

by

Vincent Quemener

Submitted in partial fulfillment of the requirements for the degree of

Philosophiae Doctor

Department of Physics

Faculty of Mathematics and Natural Sciences

University of Oslo

March 2012

Series of dissertations submitted to the
Faculty of Mathematics and Natural Sciences, University of Oslo
No. 1194

ISSN 1501-7710

Cover: Inger Sandved Anfinsen.
Printed in Norway: AIT Oslo AS.

Produced in co-operation with Unipub.
The thesis is produced by Unipub merely in connection with the
thesis defence. Kindly direct all inquiries regarding the thesis to the copyright
holder or the unit which grants the doctorate.

To my grand father

Abstract

Zinc oxide (ZnO) has been used for many years in a wide range of products, but not for its semiconducting properties. Recent improvements made in the production of ZnO generated a new interest towards this material. Indeed, the direct wide band gap (3.37 eV at room temperature) and the high exitonic binding energy (60 meV) make ZnO attractive as a transparent conducting oxide (TCO) in photovoltaic and in optoelectronic applications. In addition, the non-toxicity, the Zn availability and abundance, the possibility to grow single crystal bulk material and to deposit thin ZnO film on wide range of substrates at low temperature make this material very appealing. However, in order to reach the full potential of ZnO, several issues must be resolved, such as a full control of the inherent n-type conductivity and the achievement of p-type doping.

The work contained in this thesis is focused on the investigation of the electrical properties of hydrothermally grown ZnO and ZnO/Si heterojunctions. In particular, current-voltage (I-V), capacitance-voltage (C-V) and deep level transient spectroscopy (DLTS) techniques have been employed to characterize Pd/ZnO Schottky contact and ZnO/Si heterostructure properties. Especially, defect levels in the band gap of ZnO and at the interface of ZnO/Si heterostructures have been investigated.

Firstly, electrically active defects in hydrothermally grown ZnO have been investigated by DLTS and thermal admittance spectroscopy (TAS) through Pd Schottky contacts. Defect levels with energy positions of 0.19 (E2), 0.30 (E3) and 0.57 (E4) eV below the conduction band edge (E_c) have been observed. In addition, the different annealing conditions reveal strong influence on several defect levels. For example, E2 and E4 appear as O-rich and Zn-rich defects, respectively. Moreover, improvement made on the Pd

Schottky contacts has allowed us to explore deeper region in the band gap of ZnO by using DLTS in the temperature range up to 600K. Thus, two new defect levels have been observed with energy positions of 1.0 (E5) and 1.2 (E6) eV below E_c. These defects are strongly influenced by mechanical polishing and are tentatively assigned to vacancy type defects. Moreover, similar defect levels arise after Zn implantation, which supports the intrinsic nature of E5 and E6.

Secondly, ZnO/Si heterostructures prepared by DC magnetron sputtering and atomic layer deposition (ALD) have been investigated. X-ray diffraction (XRD) and transmission electron microscopy (TEM) have been used to investigate the structure and morphology of the ZnO layers and the interface of the heterostructures. The electronic properties of the ZnO/Si junctions have been studied by I-V, C-V and DLTS measurements. The junctions show rectifying behavior on both n-type and p-type Si and defect levels have been observed close to the interface. Moreover, the barrier heights of ZnO/Si heterostructures prepared by ALD have been investigated by I-V and C-V versus temperature. The results give an estimate of the work function of n-type ZnO, $\Phi_{ZnO} = 4.65$ eV. Finally, preliminary work has been done to compare ALD and RF magnetron sputtering and the results demonstrate that ALD is a soft deposition technique which induces less interfacial defects than sputtering.

Acknowledgments

These three years of work was a fabulous opportunity to meet, collaborate and exchange with many people, where everyone has contributed to the achievement of this thesis.

First of all, I would like to sincerely acknowledge my main supervisor Prof. Bengt G. Svensson for giving me the possibility to accomplish this thesis and for guiding me during these three years of work as well as giving me the benefit of his extraordinary experiences through out the work. Secondly, I would like to thank my co-supervisor Prof. Edouard V. Monakhov for his day to day supervision and his precious help for completing this thesis. I also want to address my gratitude to Dr. Lasse Vines, who introduced me to the equipment, helped me a lot in the experiment part, answered patiently to all my questions and had the difficult task of proofreading my first version reports. They were always available to discuss results and shared with me their significant experiences and knowledges.

I would also like to thank Mari Alnes for her contribution as co-worker in the same project, for supplying ALD samples and for sharing scientific discussion about deposition techniques and general fields.

I want to express my gratitude to my colleagues of MiNaLab for their contribution to the good working environment and for the nice moments spent together. In particular, I would like to thank Mareike Trunk, Vishnu Venkatachalapathy, Chi Kwong Tang, Helge Malmbekk, Ramon Schifano, Pekka Neuvonen, Klaus Johansen and Knut Erik Knutsen for the nice moments spent together, the scientific and general discussions, the coffee breaks, and for their good company during the weekends trips, skiing moments and conferences.

I would also like to thank my family and my friends, for their supports and encouragements along these three years of work.

Finally, I will never thank enough my dear Maelenn for her contribution and continuous support and encouragement during the ups and downs of these three years.

Contents

CONTENTS

Chapter 1

Introduction

The increase of the energy consumption and the global warming represent major issues for our future. This combined with the depletion of fossil energy sources, the development and production of clean and sufficient energy represent the largest challenge of this century. In this respect, novel semiconductors, such as zinc oxide (ZnO), may have a crucial role in the development of energy saving devices and renewable energies, e.g. photovoltaic cells.[1, 2] ZnO has been used for many years in a wide range of products,[3] but not for its semiconducting properties. Recent improvements made in growth techniques and the production of high quality single crystal ZnO generated a new interest towards this material. Indeed, one of the most interesting properties of ZnO is the direct wide band gap (3.37 eV at room temperature) making it attractive as a transparent conducting oxide (TCO)[4] in thin film photovoltaics[5] and in optoelectronic applications such as white light emitting diodes (LED).

TCOs suitable for use as thin-film transparent electrodes, require degenerated semiconductors with high carrier concentration ($>10^{20}$ cm^{-3}), low resistivity ($< 10^{-3}\ \Omega.cm$) and transmittance, in the visible part of the spectrum, higher than 80%. So far, a multitude of materials are available as TCO, and the most commonly used ones for industrial purposes are Sn doped In_2O_3 (ITO), F doped SnO_2 (FTO) and Al doped ZnO (AZO). TCOs have been used for several decades but not much studied, probably because their performances were sufficient for specific applications (e.g. flat screen, touch-sensitive screen, electrochromic window). However, in the case of photovoltaic cells, TCO may have a direct impact on the performance of the complete device, where defects and in-

terfacial layers may reduce the efficiency of the solar cells. At present time, ITO is the most industrially used TCO, mainly due to higher electrical conductivity and higher transparency compared to other TCO materials. However, the fast-growing demand for TCOs for optoelectronic devices will rise up the price of ITO due to the lack of Indium. Hence, ZnO based materials appear as a promising alternative and have gained interest due to low cost production, non-toxic elements, and the ability to exhibit resistivity comparable to ITO. Moreover, the possibility to tune the energy band gap of ZnO by introducing Cd or Mg makes ZnO suitable to be used as an active layer in the future generation of multi-junction solar cell.[6, 7]

Another property making ZnO very promising is its high exciton binding energy (60 meV) which is twice that of GaN. Thus, ZnO has a potential to be used in light emitting diodes (LEDs) and laser diodes; a large scale production of white LEDs could reduce considerably the global energy consumption and ZnO may also play a major role in this development. Other properties of ZnO such as the chemisorption capability, piezoelectricity and the possibility to dope ZnO with transition metals make ZnO suitable in a wide range of applications in gas sensors, piezoelectric and spintronic devices.[8, 9, 10]

However several issues must be addressed before extensive use of ZnO in commercial applications. ZnO is a naturally n-type semiconductor and the origin of its conductivity is still a controversy. In order to understand the native n-type origin of ZnO, a thorough knowledge of the impurities and intrinsic point defects is essential. Further, electrically active defects may dramatically affect the electrical and optical performances and the control of these defects during growth and device processing is crucial. In addition, even if achieving n-type ZnO is relatively easy, a perfect control of the doping must be pursued for applications in electronic devices. Finally, another main obstacle for extensive use of ZnO is the difficulty in achieving stable and highly conductive p-type layers and thus making p-n junctions and transistors. Several groups have reported p-type ZnO but the reproducibility, the hole concentration and the mobility are generally low. The main reason is that ZnO is 'naturally' n-type and a majority of defects play a role in compensating the p-type doping. Another reason is that only a few candidates exist as shallow acceptors for ZnO, according to theoretical predictions.

In this thesis, electrical properties of bulk ZnO and thin film ZnO have been investigated. The thesis is organized as follows: Chapter 2 introduces the semiconductor

physics relevant to the study, the defects in semiconductors and the general properties of ZnO. Chapter 3 describes the experimental techniques used in the work. Chapter 4 summarizes the work and the main results obtained. The results are structured into two parts: firstly, defect levels in the band gap of hydrothermally grown ZnO have been investigated by capacitance techniques. In particular, the results reported in Paper I and III focus on the effects of annealing conditions on defect levels. Paper II points out the effects of polishing on the defect levels in ZnO and Paper IV reports on an ion implantation study. Secondly, ZnO/Si heterojunctions prepared by sputtering and atomic layer deposition (ALD) have been investigated; the results reported in Paper V and VI focus on the investigation of interface defects between ZnO and Si, while Paper VII addresses the barrier heights of ZnO/Si junctions.

Chapter 2

Properties of ZnO

This chapter introduces a brief review of the semiconductor physics, the junction formation and the effects of defects and impurities on the properties of the semiconductors. Finally, the main properties of ZnO as transparent conducting oxide will be summarized.

2.1 Properties of semiconductors

An electron in a single isolated atom may only occupy discrete energy levels, called orbitals. When two isolated atoms approach each other, the interaction between their atomic orbitals will form new molecular orbitals known as bonding and antibonding orbitals, resulting in new energy levels. This concept of bonding and antibonding orbitals can be extended for solid-state materials, where a large number of atoms interact and the overlap of bonding and antibonding orbitals will result into continuous energy bands separated by forbidden intervals called band gaps. Electrons in a solid-state material obey the Fermi-Dirac distribution, where the probability $f(E)$ that an available state will be occupied by an electron is given by $f(E) = (1 + exp((E - E_F)/kT))^{-1}$, where E_F is the Fermi level, k is the Boltzmann constant and T is the absolute temperature. Depending on the position of the Fermi level and the band structure of the material, the materials can be classified into three types; insulators, metals and semiconductors. An insulator has the allowed energy bands either filled or empty of electrons and will

not respond to an applied electrical field, while a metal has the allowed band partially filled by electrons and responds instantaneously to an applied electrical field. A semiconductor, like an insulator, is characterized by a band gap (E_g). At $T = 0K$, the uppermost energy band below this band gap, called *valence band* (E_v), is fully occupied by electrons and the lowermost energy band above the band gap, called *conduction band* (E_c), is unoccupied. The difference with an insulator, is that electrons can be thermally excited from the valence band to the conduction band and, thus, transport current. In semiconductors, the electrical conductivity is controlled by two types of charge carriers; electrons in the conduction band (n-type doping) and holes in the valence band (p-type doping). Moreover, specific dopants can be introduced in the semiconductor in order to control the conductivity and the type of the semiconductor. By doping the semiconductor with a shallow donor impurity which donates an electron to the conduction band, the semiconductor will have an excess of negative charge carriers (n-type), while semiconductor doped with shallow acceptor impurities will have a deficit of free electrons resulting in an excess of positive charge carriers (p-type). In an ideal semiconductor without any impurities, the Fermi level is located close to the middle of the band gap and the semiconductor has low intrinsic carrier concentration controlled by the ratio E_g/kT. However, in a doped semiconductor, the Fermi level is pushed towards the conduction band or towards the valence band for n-type and p-type material, respectively.

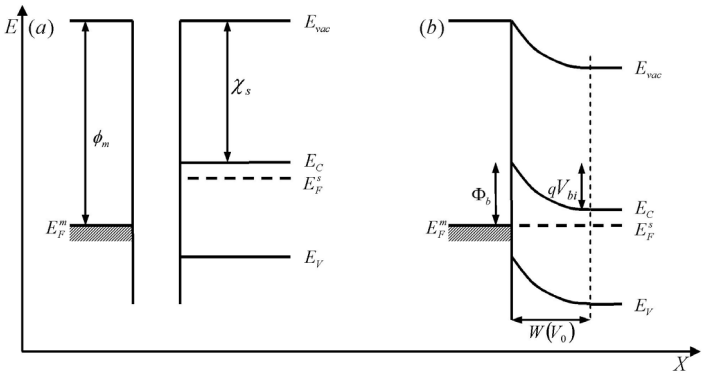

Figure 2.1: Energy band diagram of the formation of Schottky metal-semiconductor (n-type) before (a) and after perfect contact (b)

A rectifying junction is crucial for most semiconductor devices as well as a tool for electrical characterizations of physical properties of semiconductors. As described in the introduction, fabrication of ZnO p-n junctions is limited due to the lack of p-type ZnO. However, Schottky contacts on ZnO using different metals have been reported in the literature[11, 12] and recent improvements achieved on the junction have allowed the use of Schottky contacts for electrical investigation of ZnO by capacitance techniques. In the following, we limit the description to the Schottky junction, but similar considerations hold for a p-n junction.

The interruption of the periodic potential of the crystal at the surface of the semiconductor modifies the energy potential of the surface. We consider an ideal junction formation between a n-type semiconductor with an electron affinity (χ_s) and a metal with a work function (ϕ_m), where $\phi_m > \chi_s$ (see Fig. 2.1a). By depositing the metal contact onto the surface of the semiconductor, electrons from the semiconductor can lower their energy by moving towards the metal. At equilibrium, the Fermi level of the metal (E_F^m) and of the semiconductor (E_F^s) will coincide. According to the Schottky-Mott model[13], a band bending of the band edges of the semiconductor occurs, resulting in the formation of a region depleted of free charge carriers with a width W and a barrier Φ_b. The height of the barrier relative to the Fermi level is given by:

$$\Phi_b = \phi_m - \chi_s. \tag{2.1}$$

By applying bias to the metal-semiconductor junction, the difference between E_F^m and E_F^s can be manipulated. Under forward bias, E_F^s is raised, thus, the potential across the semiconductor decreases and allows electrons to flow through the junction, which leads to a positive current through the junction at a voltage comparable to the built-in potential V_{bi}. Under reverse bias, E_F^s is lowered, the potential across the semiconductor increases, yielding larger depletion region and larger electric field at the interface, and limiting the flow of electrons.

The capacitance C of the depletion region can be determined as a function of the built-in voltage and is given by the derivative of the total charge Q in the depletion region $C = dQ/dV_I$, where $V_I = V_{bi} - kT/q$. By solving the Poisson's equation $\Delta V =$

$\rho(x)/\epsilon$ with boundary conditions, where the charge density is $\rho(x) = qN_D$. For $0 \leq x \leq W$, the potential is given by:

$$V_I = \frac{qN_D}{2\epsilon}W^2, \tag{2.2}$$

where ϵ is the permittivity of ZnO, q is the elementary charge and N_D is the carrier concentration. To satisfy the charge neutrality of the junction, the total charge in the depletion region is $Q = AqWN_D$, where A is the area of the Schottky contact. Thus, combined with Eq. 2.2, the total charge becomes, $Q = A(2q\epsilon N_D V_I)^{1/2}$. Further, the capacitance of the contact can be described by two parallel capacitor plates separated by the distance W, and the capacitance of the depletion region becomes:

$$C = \frac{dQ}{dV_I} = A\sqrt{\frac{\epsilon q N_D}{2V_I}} = A\frac{\epsilon}{W}. \tag{2.3}$$

In addition, the electrical field F in the depletion region corresponds to the derivative of the potential in the depletion region and is given by $F(x) = -\frac{dV}{dx} = -\frac{qN_D}{\epsilon}(W - x)$. The capacitance of a junction is very important and represents the base for the electrical characterization techniques employed in this thesis.

Fabrication of ideal contacts remains difficult and several factors can strongly modify the properties of the junction, such as the presence of trap states and/or an insulating layer at the interface. These different factors may influence the barrier height and Eq. 2.1 may no longer be appropriated. Bardeen has developed the model further[13] to describe the barrier height, as illustrated in Fig. 2.2 where he has considered an ideal Schottky contact with an interface oxide layer with a thickness δ sufficiently thin so that charge carriers can tunnel through the interface, and with a density of interfacial states D_s homogeneously distributed in the band gap. Under these conditions, the barrier height becomes:

$$\Phi_b = \gamma(\phi_m - \chi_s) + (1 - \gamma)(E_g - \phi_0), \tag{2.4}$$

where $\gamma = \epsilon/(\epsilon + q\delta D_s)$ is a factor taking into account the oxide layer thickness and the density of states. Thus, when $\gamma \to 1$ (no interfacial states and/or no oxide layers), the barrier height is reduced to the Schottky-Mott model in Eq. 2.1. In the

other limiting case, when $\gamma \to 0$ ($D_s \to \infty$), the barrier height becomes independent of ϕ_m and χ_s and the Fermi level is pinned at an energy ϕ_0 above the valence band edge.

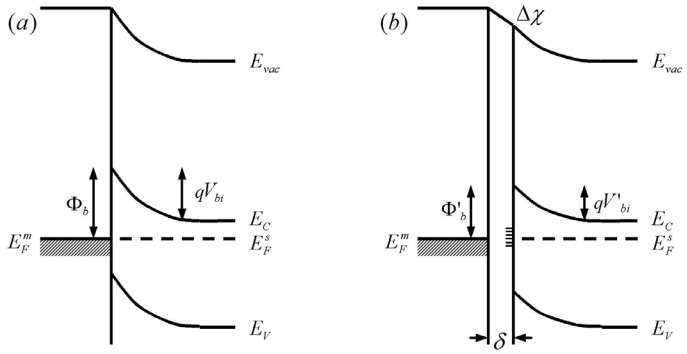

Figure 2.2: Energy band diagram of metal-semiconductor for an ideal contact according to Schottky model (a) and with interface oxide layer with a thickness δ and a density of states D_s according to Bardeen model (b).

2.2 Native defects and impurities

Defects are crucial to the electrical properties of a semiconductor material. A perfect single crystal semiconductor without any defects will have limited free carriers and thus a low intrinsic conductivity. Therefore, defects are necessary to supply charge carriers in the semiconductor and make the material conducting. The control of the introduction of specific defects allows us to tune the properties of the semiconductor. However, unintentional introduction of defects occurs and may drastically affect the electrical characteristics of the material. Thus, defect control is a key challenge.

Defects can be categorized in function of their dimensions, which are large three dimensional (3D), planar (2D), line (1D) and point (0D) defects. Here we limit the discussion to point defects, since it is the topic of the thesis. In the crystal, defects distort the periodic potential and may introduce additional electronic states. Depending on the energy position of the electronic states, the defects can be either electrically active or inactive. An electrically active defect will introduce additional discreet levels

in the electronic band gap of the semiconductor. The electrically active defects have different characteristics depending on the location of their energy states relative to the conduction and the valence band edges. These defects can influence the electrical properties of the semiconductors. States located close to the conduction and valence band are called shallow levels, which are usually used for doping of the semiconductor. States called deep levels reside further away from the band edges and may act as generation/recombination centers.

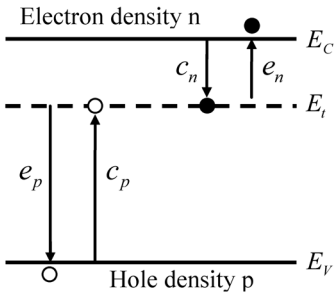

Figure 2.3: Illustration of the capture ($c_{n,p}$) and emission ($e_{n,p}$) processes of electrons and holes from the conduction band and valence band, respectively, for a defect level.

Consider a defect having a level in the band gap with a trap concentration N_t and an energy position E_t below the conduction band edge. According to the Shockley-Read-Hall statistics[14, 15], electrons and holes from the conduction and valence band, respectively, can be captured or emitted by the defect level (see Fig.2.3). This process is controlled by the capture ($c_{n(p)}$) and emission rates ($e_{n(p)}$). Thus, the fraction of the state occupied by carriers, n_t, is determined by the competition between the emission and capture processes, described as $dn_t/dt = (c_n + e_p)(N_t - n_t) - (c_p + e_n)n_t$. The capture rate per unoccupied trap can be written as $c_{n(p)} = \sigma_{n(p)}\nu_{th,n(p)}$, where $\sigma_{n(p)}$ and $\nu_{th,n(p)}$ are the capture cross section and the thermal velocity of an electron or a hole, respectively. The emission rate of electrons and holes are defined by the Fermi-Dirac distribution and given by:

$$e_n = \sigma_n \beta T^2 exp\left(-\frac{E_c - E_t}{kT}\right), \tag{2.5}$$

where $\beta = \sqrt{\frac{3k}{m_n^*}} 2 \left(\frac{2\pi m_n^* k}{h^2}\right)^{3/2}$ is a factor independent of the temperature. m_n^* is the electron effective mass in ZnO and h is the Plank constant. Depending on the position of the defect in the band gap and the values of the emission and capture coefficients, different processes will dominate. For example, generation of electrons occurs when e_n and e_p dominate, while recombination occurs when c_n and c_p dominate. The main processes are summarized in the table 2.1.

Table 2.1: Overview of the main processes dependent of the values of emission and capture coefficients.

Process	dominant coefficients
Trapping	$e_{n(p)} \gg e_{p(n)}$ and $c_{n(p)} \gg c_{p(n)}$
Generation	$e_n \gg c_n$ and $e_p \gg c_p$
Recombination	$c_n \gg e_n$ and $c_p \gg e_p$

As previously described in section 2.1, an electric field is present through the depletion region of a Schottky diode. The potential well of a defect in the depletion region can be distorted by the electric field through the Poole-Frenkel effect. As illustrated in Fig. 2.4, when the Poole-Frenkel effect occurs, the barrier height is lowered by the electric field F, according to Frenkel[16] by the amount $\Delta E_T = 2\left(q^3 F/\epsilon\right)^{1/2}$. Thus, in an n-type semiconductor, if a defect level shows a dependence of its energy position with the square root of the electric field, the defect will be interpreted as a donor-type.

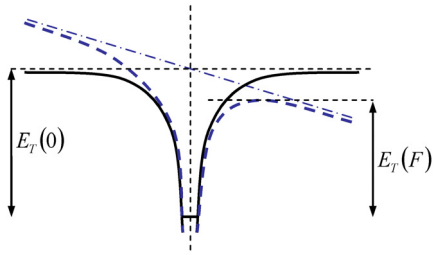

Figure 2.4: Mechanism of Poole-Frenkel effect. The solid line is the potential well of a defect without electrical field with a barrier height $E_T(0)$. The dashed line shows the distorted potential well by an electric field F with a lowered barrier height $E_T(F)$ for a charged defect.

2.3 Basic properties of ZnO

ZnO[1, 2] crystallizes, at ambient pressure, in the hexagonal wurtzite structure (see Fig.2.5), belonging to the space group $P6_3mc$. The hexagonal unit cell is constituted by two interconnecting inversed tetrahedral sub-lattices shifted along the [0001] direction (c-axis) with lattice parameters of a = 3.25 Å and c = 5.21 Å. In addition, the wurtzite structure has no inversion symmetry along the c-axis. This coupled with the ionic nature of the bonds and the ratio $c/a = 1.603$ which deviates from the ratio of an ideal hexagonal structure ($c/a = \sqrt{8/3} = 1.633$), yield a high crystal polarity between the two opposite faces along the c-axis, i.e., an electrical potential occurs between the two faces (0001) and (000$\bar{1}$) which results in a strong piezoelectric effect. These two polar faces are labelled Zn-face and O-face respectively, depending on the surface specie. Thus, the difference in polarity may influence the experimental results on the two surface terminations, e.g., barrier height formation of a Schottky contact.[12, 17]

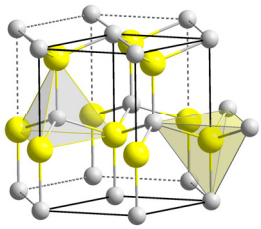

Figure 2.5: Hexagonal wurtzite structure of ZnO.

ZnO has a direct and wide band gap of 3.37 eV at room temperature in the wurtzite structure. ZnO exhibits a high transparency and a natural n-type conductivity. Thus, the combination of these properties makes ZnO very attractive as a TCO. In addition, ZnO has a high exciton binding energy of $\sim 60\,meV$ (compared to GaN, $\sim 25\,meV$), which, combined with the large band gap, give a high potential as a material for light emitting devices operating in the white, blue and ultra-violet wavelength regimes.

Some of the main properties of ZnO and their values, relevant to the thesis, are compiled in the table 2.2, taken from Refs [9] and [1]. Some of the values are uncertain, in particular for p-type ZnO where the hole effective mass differs in the literature.

Table 2.2: Overview of relevant parameters of ZnO.

Property	Value
Energy gap, E_g	$3.4371 - (5.05 \times 10^{-4} T^2/900 - T)$
Exciton binding energy	$60\, meV$
Relative permitivity, $\epsilon_{r\|c}$	8.91
$\epsilon_{\infty\|c}$	3.66
Electron effective mass, m_n^*	$0.24 m_0$
Hole effective mass, m_h^*	$(0.58 - 0.78) m_0$
Richardson constant, A^*	$32\, AK^{-1}cm^{-2}$
Bulk hardness	$5.0 \pm 0.1\, GPa$

In order to reach the full potential of ZnO, several technological advances are necessary, where the main challenges are: (i) controlling the natural n-type conductivity and (ii) achieving stable and low resistive p-type ZnO.

So far, the origin of the native n-type conductivity is still under debate. Originally, the n-type conductivity was attributed to intrinsic defects, such as Zinc interstitial Zn_i and Oxygen vacancy V_O, but recent works have demonstrated that these hypothesis may not be correct. V_O behaves as a double donor and has a low formation energy, but DFT calculations show that V_O is a deep donor and cannot contribute to the n-type doping.[18, 19] Zn_i acts as a shallow donor, however, its formation energy is high in n-type ZnO which limits its ability to control the n-type conductivity. Unintentional impurities acting as shallow donor may also contribute to the native n-type doping. Hydrogen, for example, is present in high concentration in ZnO, irrespective of the growth condition. H in interstitial site or in a oxygen vacancy acts as shallow donor.[17, 20, 21, 22] Other impurities, such as Al, Ga and Si have also been suggested to explain the native n-type doping.[23, 24] However, the presence of these impurities depends on the growth methods, so a combination of intrinsic and impurity related shallow donors for explanation of the native n-type doping is appealing.

Even if the n-type doping is readily accessible, the control of the n-type doping concentration remains difficult and varies substantially with the growth processes, e.g. ZnO wafers from the same growth process have native carrier concentration varying

from $\sim 5 \times 10^{16}\ cm^{-3}$ to $5 \times 10^{17}\ cm^{-3}$. However, doping ZnO with impurities such as Ga or Al has also demonstrated the possibility to reach highly conductive material with high carrier concentration $> 10^{21}\ cm^{-3}$ and low resistivity $< 10^{-4}\ \Omega.cm$,[25, 26] which is crucial for TCO applications.

Achieving p-type ZnO represents another major challenge.[27, 28] Similar behavior has been demonstrated in several wide band gap semiconductors where one doping can be easily achieved while the opposite is difficult. For example, ZnO and GaN favor n-type doping, while ZnTe favors p-type. The main difficulties in achieving p-type ZnO arise from: i) deep donor defect centers, which are not responsible of the n-type conductivity, will compensate the p-type doping. ii) Only a few candidates have suitable properties to be a shallow acceptor in ZnO. iii) Several of the potential dopants have a low solubility. The main p-type candidates are group-I elements (Li, Na and K) substituting for Zn sites or group-V elements (N, P and As) substituting for O sites. However, most of these dopants can also act as deep acceptors and do not contribute to the p-type conductivity. For example, group-I elements are stable in interstitial sites and will act as donors and compensate the p-type doping. However, several studies have reported on the fabrication of p-type ZnO but the stability and the reproducibility have shown to be difficult.[29, 30] Thus, related to the attempts of making p-type material, a thorough understanding and control of the native defects present in ZnO and of the n-type doping must be achieved.

Electronic devices and electrical investigations of ZnO by junction spectroscopy techniques require rectifying contacts. Therefore, ZnO Schottky and Ohmic contacts have been extensively studied over the past decades[11, 12], and an improvement of high quality Schottky contacts have been achieved.[31, 32], However, several aspects of the Schottky barrier are not fully understood and the stability of the contacts remains not completely controlled. Depending on the crystal orientation, the surface preparation and the condition of metal deposition, the diode properties can vary significantly. For example, using Pd Schottky contacts, the reported barrier heights vary from 0.55 eV[33] to 1.2 eV.[34] Thus, achieving Schottky contacts with sufficient quality for a full understanding and control of the barrier height represents a challenge.

Different techniques exist to growth single crystal ZnO bulk material and three main processes are employed; melt growth[35], vapor phase[36] and hydrothermal growth.[37]

Hydrothermally grown ZnO (HT-ZnO) wafers obtained from SPC-Goodwill have been used in this thesis. In the hydrothermal growth process, high purity ZnO is dissolved in LiOH/KOH base solution in the bottom part of a closed autoclave heated up to temperature of $300 - 400°C$ and with a pressure in the 70-250 MPa range. In the upper part of the autoclave, high purity seeds of ZnO crystals are suspended by Ti wires. A temperature gradient of $\sim 20°C$ is maintained between the dissolution part (bottom) and the growth part (upper part). The lower temperature will favor the growth where a growth rate of $\sim 0.2\, mm/day$ is typically obtained. The growth rate can be improved by using several seeds in the same autoclave in order to scale up the growth process and reduce the cost. Thus, hydrothermal growth is expected to be an economically viable method and leads to high quality ZnO monocrystals. However, due to the mineralizers LiOH and KOH used during the growth of HT-ZnO, impurities like Li and K are incorporated in the material with concentration of $\sim 10^{17}\, cm^{-3}$. In particular, Li can have a huge influence on the electric properties of ZnO. Indeed, Li is an amphoteric impurity and can be a donor or acceptor, depending on its atomic configuration. Thus, Li can act as a self-compensating defect often resulting in a high resistivity HT-ZnO ($\sim 1000\, \Omega.cm$). In addition, depending on the purity of the precursors and growth chamber, other impurities can be present in ZnO, like Al, Fe, Si and Mg with lower concentrations.[38]

As mentioned in the introduction, ZnO attracts much attention in thin film technologies with a wide range of applications such as photovoltaic cells, light emitting diodes, laser diodes and transparent devices. For example, degenerated ZnO can act as transparent front contact to the emitter or even as the emitter itself if a rectifying contact occurs between ZnO and the base. Thus achieving and studying the behavior of ZnO/Si heterojunctions with high quality contacts are important for solar cells applications. Thin film of ZnO can be prepared by a wide variety of deposition techniques and the main ones used are pulsed laser deposition (PLD),[39, 40, 41] sputtering,[25, 41, 42] metal-organic chemical vapor deposition (MOCVD)[1, 41] and atomic layer deposition (ALD).[42, 43] ZnO can be deposited on wide range of substrates (Sapphire, glass, Si) at relatively low temperature compared to other wide band gap semiconductors, which makes ZnO attractive for low cost manufacturing.

Sputtering represents one of the most scalable techniques to deposit ZnO thin films

with low substrate temperature, high deposition rate and good thickness uniformity. However, the crystalline quality can be low compared to other techniques, and ZnO films have generally a columnar structure with polycrystalline grains oriented preferentially along the c-axis. Further, the electrical properties obtained with Al-doped sputtered ZnO films are similar compared with ITO at comparable carrier concentration ($> 10^{21}\ cm^{-3}$) and resistivity ($< 10^{-4}\ \Omega.cm$).[25, 44]

ALD represents a high interest for depositing high quality ZnO with a good control of the thickness and uniformity on large surface area. Moreover, the excellent conformality combined with the atomic precision of deposition allow to develop 3D nanostructured solar cell architectures. However, several aspects have to be improved such as the crystal structure and the purity of the ZnO layer. In particular, H is present in high concentration and can affect the electrical properties.[45] Thus, the control of free carriers in the material remains difficult and ZnO thin film with donor concentration of $\sim 10^{20}\ cm^{-3}$ and resistivity of $\sim 10^{-3}\ \Omega.cm$ for undoped ZnO are commonly reported in the literature.[42, 43, 46] The ZnO films show polycrystalline structure with preferentially orientation depending on the growth temperature.[42]

In thin film polycrystalline ZnO, the electron mobility remains relatively low compared to that in bulk monocrystalline samples, where mobility values higher than $200\ cm^2V^{-1}s^{-1}$ are achieved for vapor phase grown material at 300K.[36] However, very promising results have been obtained for thin film epitaxial layers of ZnO grown by PLD[47] and Molecular Beam Epitaxy (MBE)[48] yielding electron mobilities around $150\ cm^2V^{-1}s^{-1}$ at RT.

In both bulk and thin film ZnO, intrinsic and impurity related defects are present and need to be identified and controlled. Several different types of point defects exist in ZnO (see Tab. 2.3) and can be ordered in three categories; (i) Zinc and Oxygen vacancy (V_{Zn} and V_O), (ii) Zinc, Oxygen and impurity (X) in interstitials sites (Zn_i, O_i and X_i) and (iii) substitutional with Zn_O, O_{Zn}, X_{Zn} and X_O. More complicated defects can be found with the combination of several defects which form clusters.

Defect levels in the band gap can be characterized by optical and electrical techniques. Optical characterization techniques such as photoluminescence (PL)[49, 50] and cathodoluminescence (CL)[51, 52] do not require contacting of the sample and

Table 2.3: Overview of main possible point defects in ZnO

	Intrinsic	Extrinsic
Vacancy	V_O(D), V_{Zn}(A)	
Interstitial	Zn_i(D), O_i(N,A)	X_i(A,D)
Substitutional	$Zn_O(D)$, $O_{Zn}(A)$	X_O, X_{Zn}(A,D)

have been extensively used for ZnO; they give information about various charge carrier transitions, such as band-to-band, localized-state-to-band as well as between interval states of a defect. However, in this thesis defects in the band gap have been investigated mainly by junction spectroscopy techniques such as deep level transient spectroscopy (DLTS) and thermal admittance spectroscopy (TAS). Several defect states have been reported in the literature using junction spectroscopy and some of these have similar properties. The main reported defect levels observed in ZnO are summarized in table 2.4. Despite a substantial effort, their origins remain unclear and are still a subject of debate. In particular, the defect level localized at 0.3 eV below the conduction band edge, generally labelled E3, is the most reported defect in ZnO. E3 is present in most ZnO materials, irrespective to the growth techniques used. This level has commonly been assigned to V_O. However, the weak dependence of E3 on electron and ion irradiations contradicts the assignment to V_O[53]. An origin like the second ionization of Zn_i has also been proposed[54]. However, the high formation energy of Zn_i in n-type material limits its concentration and therefore limits its influence on the n-type doping. Impurities such as Ni and Fe[55] have also been proposed, but the fact that E3 is independent of the growth technique leads the assignment to an intrinsic defect, supported by SIMS analysis[38]. In addition, it has also been proposed that E3 is the association of at least two overlapping defect levels[56, 57], with at least one related to V_O.

Most recently, efforts have been made to realize highly stable Schottky contacts which allow to explore deeper region of the band gap of ZnO by DLTS. Thus, defect levels with energy positions in the 0.8-1.2 eV range below E_c have been reported.[58, 59] These defects show strong dependence on irradiation/polishing processes and have been assigned to extended defects and vacancy related defects.

ZnO is a soft material, with a hardness of $\sim 5\,GPa$. The mechanical properties have been investigated by spherical indentation techniques which induced extensive

damages[1, 60] up to 300 nm in the bulk of ZnO. Thus, mechanical processes, such as polishing, may cause extended defects in the region close to the surface of ZnO and influence the electric properties. The polishing effects on the properties of ZnO have been studied by photoluminescence and positron annihilation spectroscopy (PAS) which show formation of open-volume defects in the region close to the surface.[61] In this thesis, extended defects induced by polishing have been revealed by DLTS measurements, as discussed in paper II.

Table 2.4: Overview of the main defect levels observed in n-type ZnO by junction spectroscopic techniques.

$E_c - E_t$ (eV)	σ_{na} (cm^2)	Growth method	Measurement technique	Tentative origin
0.013[57]	-	HT	TAS	unknown
0.03[62, 63]	-	HT	TAS	H related complex[62], Zn_i[64]
0.03-0.4[64]	$10^{-17} - 10^{-15}$	MG	CDLTS	After irradiation assigned to H or Zn_i[64]
0.05[57, 62, 63, 65]	-	HT	TAS	Al related[62]
0.10[66]	10^{-18}	VP	DLTS	unknown
0.12[66]	10^{-13}	VP	DLTS	unknown
∼**0.20**[24, 67]	10^{-16}	HT,VP	DLTS	associated to Li impurities[68, 69, 70], promoted by O-rich conditions,[1]
∼**0.30**[24, 53, 57, 62, 63, 65, 66]	$10^{-16} - 10^{-15}$	HT,VP,MG	DLTS,TAS	Most important defect, assigned to V_O[53], Zn_i[54] and also Ni or Fe related[55], Does not respond to irradiation or annealing atmosphere, stable up to $\sim 1300°C$,[2]
∼**0.55**[66, 67]	$10^{-13} - 10^{-12}$	HT,VP	DLTS	intrinsic defect like V_O[67], increase after irradiation[71], promoted by Zn-rich conditions,[3]
∼0.70	$10^{-15} - 10^{-12}$	HT	DLTS	unknown
∼**1.00**[58, 59]	$10^{-13} - 10^{-12}$	HT,VP,MG	DLTS	Increase after irradiation and polishing,[4]
∼**1.20**[59]	10^{-15}	HT	DLTS	Increase after irradiation and polishing,[5]

HT, MG and VP correspond to Hydrothermal, Melt Grown and Vapor Phase methods, respectively.

[1,3] Reported in papers I and III. The formation/suppression of these defects correlates with the Zn- and O-rich annealing conditions.
[2] Reported in Papers I-IV.
[4,5] Reported in Papers II and IV. The defects occur after polishing and Zn implantation which suggest intrinsic nature.

Chapter 3

Experimental methods

This chapter summarizes the main experimental techniques used in this thesis. Current versus Voltage and Capacitance techniques are mainly employed to investigate the electrical properties of the contacts. Deep Level Transient Spectroscopy (DLTS) and Thermal Admittance Spectroscopy (TAS) are capacitance techniques used to characterize defect levels in the band gap of the semiconductor. In addition, a brief review of Hall effect measurements and Secondary Ion Mass Spectrometry (SIMS) will be given.

3.1 Current-Voltage (I-V)

Current versus Voltage (I-V) measurements give information about the metal/semiconductor contact behavior. In the case of DLTS investigations, a depletion region is required, so good Schottky behavior of the metal/ZnO contact and a high robustness of the barrier height of the junction under reverse bias are crucial. Thus, I-V allows to test the rectifying behavior of the desired diode. In addition, I-V measurement gives information about the electrical transport mechanisms and several properties of the junction, such as the barrier height. By determining the barrier height, one can also extract some basic parameters such as the work function and the electron affinity of ZnO. Figure 3.1 shows a typical example of I-V measurements for a Pd Schottky contact on HT-ZnO. The junction has a diode like behavior with a rectification of 4-5 orders of magnitude between -1V and +1V. Assuming that the current I through a Schottky

contact is controlled by the thermionic emission process, and for $V > 3kT$ the forward current versus voltage is described by:

$$\frac{I}{I_s} = exp\left(-\frac{qV_{eff}}{nkT}\right) - 1, \tag{3.1}$$

where I_s is the reverse saturation current, n is the ideality factor, $V_{eff} = V - IR_s$ is the effective voltage and R_s is the series resistance of the equivalent electrical circuit of a Schottky contact. Eq. 3.1 allows to estimate R_s and is given by $G = \frac{\partial I}{\partial V} = \frac{qI}{nkT}(1 - GR_s)$, where G is the conductance. Thus, R_s is obtained from the linear plot G/I versus G (see inset in Fig.3.1). The reverse saturation current is related to the barrier height Φ_{b0}^{I-V} and is given by:

$$I_s = A^* A T^2 exp\left(-\frac{\Phi_{b0}^{I-V}}{kT}\right), \tag{3.2}$$

where A is the contact area and $A^* = (4\pi m^* q k^2)/h^3$ is the Richardson constant given from the thermionic emission theory. The ideality factor is a measure of the contact quality. For an ideal Schottky contact, described by thermionic emission theory, the ideality factor is close to unity. The presence of defects and an oxide layer at the interface will result in an increase of the ideality factor. In addition, other current transport mechanisms, such as generation/recombination in the depletion region and carrier tunneling through the barrier, can influence the ideality factor.

Temperature dependent I-V measurements are valuable to extract information about the electrical transport mechanisms. By rewriting Eq. 3.2 to the form $\ln(I_s/T^2) = \ln(A^* A/I_s) - \Phi_{b0}^{I-V}/kT$, the barrier height Φ_{b0}^{I-V} and the Richardson constant A^* can be determined experimentally from a linear plot of $\ln(I_s/T^2)$ versus $1/kT$. A^* is very sensitive to the quality of the Schottky contact, with strong influence from defects and/or interfacial oxide layer. Further, a deviation of A^* from theoretical values may also indicate an inhomogeneous barrier height.[72]

In this thesis, for the investigation of bulk HT-ZnO, I-V has been employed at room temperature to verify the desired Schottky behavior and typically Pd-Schottky contacts with 4-5 orders of magnitude of rectification have been achieved. For investigation of

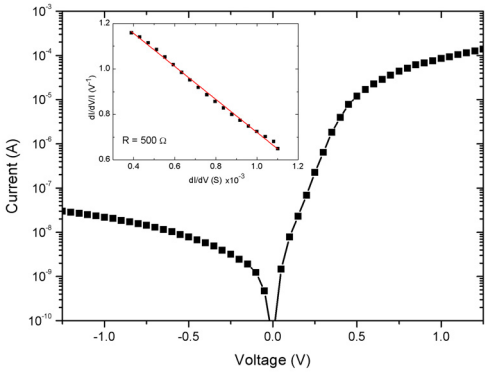

Figure 3.1: I-V measurement carried out at room temperature for Pd Schottky contact on HT-ZnO. The insets shows the G/I versus G linear plots for determining R_s.

the ZnO/Si heterojunction, I-V has been extensively used as a function of temperature to deduce the barrier height and the work function of ZnO.

3.2 Capacitance-Voltage (C-V)

Capacitance versus voltage (C-V) measurement represents, together with I-V, one of the most fundamental technique for investigating a p-n junction or a Schottky barrier. C-V gives information on the effective carrier concentration versus depth in the semiconductor and the barrier height of the junction Φ_{b0}^{C-V}.

By rewriting Eq. 2.3, the capacitance is related to the effective carrier concentration of the semiconductor by:

$$\frac{1}{C^2} = \frac{2}{A^2 \epsilon q N_D} \left(V_I + V_{rb}\right). \tag{3.3}$$

In the case of a uniform doping concentration, the effective carrier concentration can be determined experimentally from the slope of the linear fit of C^{-2} versus the applied voltage (V_{rb}) and V_I is given by the intercept of the V-axis (see Fig. 3.2a). Therefore, the barrier height can be extracted and is given by:

$$\Phi_{b0}^{C-V} = V_I + \frac{kT}{q} + \xi, \tag{3.4}$$

where ξ is the distance between the Fermi level position and the conduction band edge ($\xi = E_C - E_F$). Moreover, from C-V measurements, we can obtain information about the width of the depletion region and about the profile of doping concentration (see Fig. 3.2b). Thus, the effective carrier concentration profile at a depth W is given by[73]:

$$N_D(W) = \frac{C^3}{q\epsilon A^2} \left(\frac{\partial C}{\partial V} \right)^{-1}. \tag{3.5}$$

For instance, the effective carrier concentration gives information about the presence of defects which can compensate and/or passivate the dominant dopant, e.g. defects close to the surface will shift the depletion region deeper in the material.

For the investigation of bulk HT-ZnO, C-V has been employed at room temperature to measure the effective carrier concentration and the doping profile. For the investigation of ZnO/Si heterojunctions, C-V has been used to determine the temperature dependence of the barrier height Φ_{b0}^{C-V}.

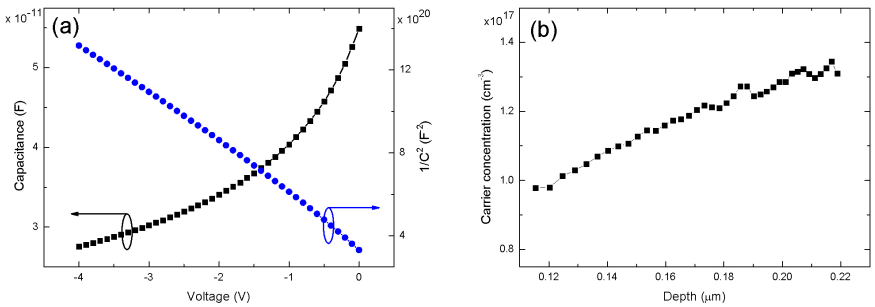

Figure 3.2: Example of C and $1/C^2$ versus Voltage measurements (a) and the corresponding effective carrier concentration profile (b) of Pd Schottky contact on HT-ZnO

3.3 Deep Level Transient Spectroscopy (DLTS)

Deep level transient spectroscopy (DLTS)[74] is a powerful technique for detecting electrically active defects in the band gap of semiconductors. DLTS gives quantitative information on the position in the band gap, the apparent capture cross section and the concentration of the defect level. The method is based on the measurement of a capacitance transient $C(t) \propto \exp(-e_n t)$ of the junction due to the emission of carriers trapped by a defect level in the depletion region (see Chapter 2.2). A DLTS cycle is based on a sequence of bias voltage alternatively fixed between a large and a small voltage during a temperature scan. We consider a Schottky contact on a n-type semiconductor which contains a deep acceptor type trap of concentration N_t, where $N_t \ll N_D$. The DLTS cycle can be described in three steps (see Fig. 3.3):

(1) At the start of the DLTS cycle, a large reverse bias is applied, so that the depletion region has a width $W(V_{rb})$ and all the traps in the depletion above the Fermi level are empty. λ, given by $\lambda = \sqrt{\frac{2\epsilon(E_c - E_t)}{qN_d}}$, corresponds to the width of the region where the defect level is below the Fermi level, so that remains filled. Thus, DLTS measurement probes a region extending to $W(V_{rb})$ - λ.

(2) A filling pulse is applied to reduce the voltage. This bias pulse reduces the depletion width to $W(V_0)$ and fills the traps below the Fermi level in this region.

(3) After the filling pulse, the reverse bias is returned to its original value in step (1). At t_0, the filled traps are again above the Fermi level and the depletion region increases to $W'(V_{rb})$, slightly larger than $W(V_{rb})$ because the charge density in the depletion region is lower than in (1). At $t_0 + t$, the filled traps start to emit carriers to the conduction band by means of the emission process given by Eq. 2.5, which results in an increase of the charge density in the depletion region and the depletion region width returns to $W(V_{rb})$.

The emission of carriers is measured by the transient of the junction capacitance. This transient can be described by an exponential decay, proportional to the emission rate of trapped carriers. The procedure is then repeated (steps 1-3) while varying the temperature and a DLTS spectrum is built by measuring the capacitance transient at each temperature. Figure 3.4 illustrates the DLTS construction by measuring the

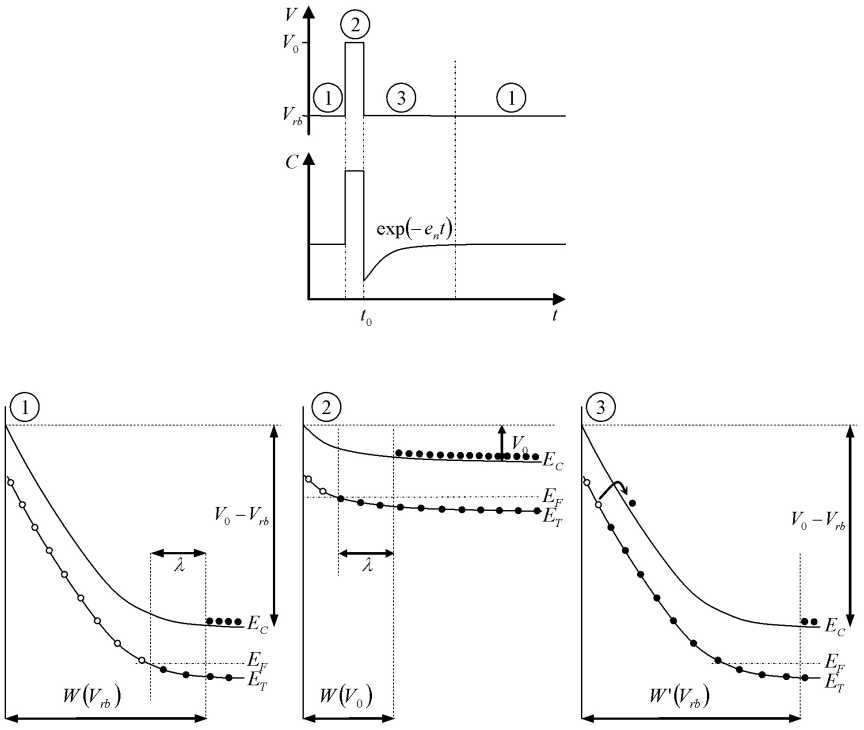

Figure 3.3: Illustration of the DLTS procedure of a Schottky contact on a n-type semiconductor having one defect level with energy position E_t below the conduction band E_c. The DLTS measurement is separated in three steps; (1) Reverse bias, (2) filling pulse and (3) charge carrier emission.

capacitance transient at two separate times (t_1 and t_2) for different temperatures. A defect in the depletion region will result in a peak in the DLTS spectrum where the peak maximum position corresponds to the emission rate from the defect level.

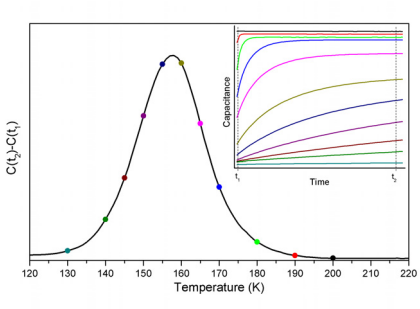

Figure 3.4: Implementation of a DLTS spectrum resulting from the transient capacitance difference measured by means of a double-boxcar with two fixed times t_1 and t_2 at different temperatures.

By varying the length of the time to measure the capacitance transient, called time window, the peak is shifted in temperature giving a set of DLTS spectra with different time windows. The variation of the time window is useful and allows investigation of a wide range of defect levels, e.g detection of levels close to midgap, while scanning over a limited temperature range. In the present case, a lock-in weighting function is applied to the capacitance transient and each time window corresponds to a specific emission rate. Thus, one DLTS spectrum is built for each time window during the same temperature scan when recording the full transient.

A defect level will generate a set of DLTS peaks versus temperature with their corresponding emission rates (T, $e_n(T)$), and an Arrhenius plot can be constructed by rewriting Eq. 2.5 to the form $ln\left(e_n/T^2\right) = ln\left(\beta\sigma_{na}\right) - \Delta H/kT$. The activation energy enthalpy (ΔH) and the apparent capture cross section (σ_{na}) of a defect level can be extracted from the slope of the line and the intercept at $1/T = 0$, respectively. Figure 3.5 shows an example of DLTS spectra of HT-ZnO for 6 different time windows with one main defect in the 140-200K temperature range. The inset shows the corresponding Arrhenius plot of the observed defect level, and the energy position and apparent capture cross section are 0.30 eV and $2 \times 10^{-15}\ cm^2$, respectively.

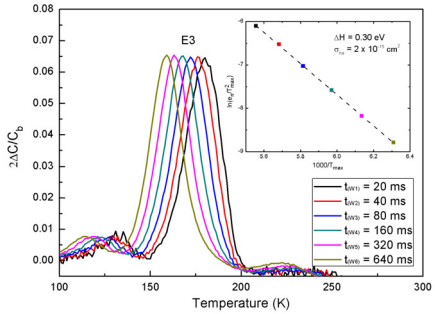

Figure 3.5: DLTS spectra for six different rate windows in the $(20 - 640ms)^{-1}$ range.

The peak amplitude of a DLTS signature is proportional to the trap concentration. If we assume a small trap concentration ($C(V_0) \gg C(V_{rb})$), the change in the depletion region width will be insignificant during the charge carriers emission, so that the emission can be described by a simple exponential decay. Further, if the trap density is uniformly distributed in the material, the relation between the trap concentration and the capacitance transient is given by:

$$\frac{N_t}{N_d} = 2\frac{\Delta C}{C_{rb}}. \tag{3.6}$$

Thus, DLTS is a very sensitive technique which allows detection of defects with concentration less than 0.01% of the free carrier concentration. However, due to the assumptions stated above, an appropriate quantification requires that the defect concentration does not exceed $\sim 10\%$ of the doping concentration.

3.4 Thermal Admittance Spectroscopy (TAS)

Thermal admittance spectroscopy (TAS)[73, 75, 76] is also used to investigate defect levels in the band gap and is also based on the temperature dependence of the charge carrier emission rate by defects (see Eq. 2.5). The measurement principle is to monitor the capacitance (C) and conductance (G) of a rectifying junction for different measurement frequencies within a temperature range. A small AC signal with frequency (f) is

applied during the temperature scan and used in order to fill the trap levels. For an appropriate temperature, the trap can emit the carrier when it crosses the Fermi level, which results in a capacitance step ΔC and a peak in $G/2\pi f_T$ equal to $\Delta C/2$.

Figure 3.6(a) shows the capacitance and conductance versus temperature of a Schottky contact on HT-ZnO. Two main levels are observed in the 30-60K and 200-300K temperature ranges, labelled D1 and E3, respectively. The shallower level observed in the 30-60K temperature range corresponds to the freeze out of the main donor level and at temperatures below the freeze out the material acts as an insulator.

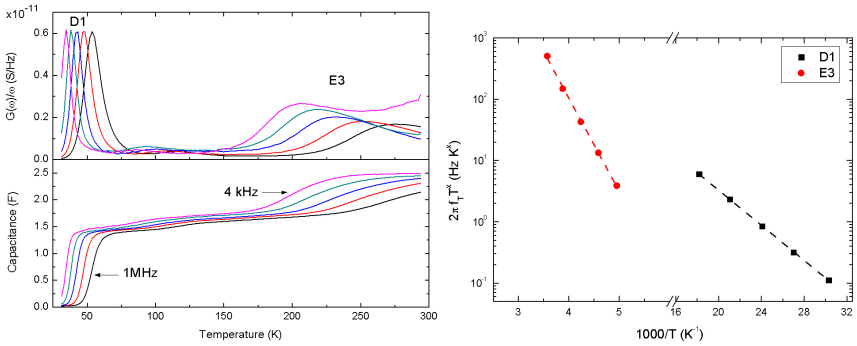

Figure 3.6: (a) Conductance and capacitance versus temperature obtained for a Schottky contact on HT-ZnO. (b) Arrhenius plot for the two defect levels D1 and E3. The temperature exponent x is $-2/3$ for the freeze out level (D1) and -2 for the level E3.

At the peak maximum (T_{max}), the emission of trapped charge carriers relates to the frequency of the AC signal, and by using a set of different frequencies, one can determine the energy position of the defect level according to the equation:

$$\frac{2\pi f_T}{T_{max}^x} \propto \exp\left(-\frac{\Delta H}{kT_{max}}\right), \tag{3.7}$$

where f_T is the frequency of the AC signal. If the main donor is monitored, x depends on the variation of the mobility with temperature during freeze out. If the freeze out occurs at low temperature, x equals 3/2.[76] For other defect levels, x is considered to be equal to 2. Figure 3.6(b) shows the Arrhenius plot for the defects D1

and E3 and their energy positions, determined from Eq. 3.7, are found to be 30 meV and 0.3 eV below E_C, respectively.

The contribution of defect levels from the depletion region can also be investigated by thermally stimulated capacitance (TSCAP) measurements.[73, 77] In that case, a reverse bias is applied at room temperature to the junction and the sample is cooled down to low temperature. A TSCAP spectrum, measured during heating up by keeping the reverse bias constant, shows only one defect level, D1(see Fig. 3.7). If a short filling pulse is applied at low temperature and then TSCAP is measured during heating up with a reverse bias, two extra capacitance steps are recorded and are independent of the AC probe frequency (see Fig. 3.7). These two capacitance steps correspond to the thermal emission of electrons trapped by two defect levels (E2 and E3) in the bulk of the depletion region during the filling pulse at low temperature. The activation energies of the two defect levels can be determined by varying the heating rate[73] or by measuring the capacitance versus time at several fixed temperatures around the capacitance step, as performed in the paper I.

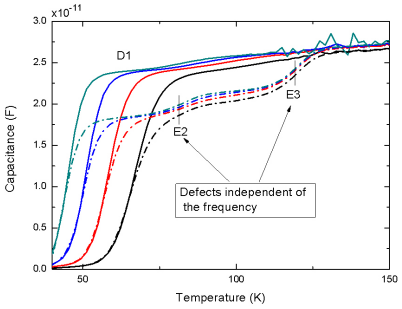

Figure 3.7: Capacitance versus temperature for Pd Schottky contact on HT-ZnO with a reverse bias of -3 V during heating up without (solid line) and with (dashed line) applying a filling pulse to zero bias voltage at 30 K. The measurements were conducted using four different AC probe frequencies.

These techniques are useful for investigation of shallow defect levels. Further, compared with DLTS, these techniques have less limitation on the maximum defect concentration to be studied, but the sensitivity is lower than for DLTS.

3.5 Hall effect measurement

Hall effect measurements are used to determine the resistivity ρ of a conducting material as well as the concentration n_H and mobility μ_H of charge carriers. For the investigation of ZnO, this technique is very useful since only Ohmic contacts are needed and high quality Ohmic contacts are easier to form than rectifying contacts.

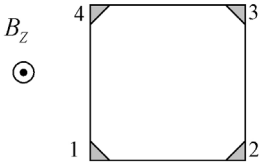

Figure 3.8: Illustration of the sample used in this thesis with the 4 Ohmic contacts.

The basis of the Hall effect can be described by considering a flat square sample with 4 Ohmic contacts at the corner of the sample (see Fig. 3.8). A current I is applied from contacts 1 to 3, which induces a flow of charge carriers. In the case of a n-type semiconductor, the majority carriers (electrons) will flow in the opposite direction of I. A magnetic field B_z applied perpendicularly to the plane in Fig. 3.8 will deflect charge carriers from the direction of contact 4 to 2 due to the Lorentz force. Thus, measurement of the current between 2 and 4 with and without a magnetic field allows a determination of the carrier concentration, n_H, according to[73]:

$$V_H = (V_{42})_{B=B_z} - (V_{42})_{B=0} = \frac{IB_z}{n_H d}, \tag{3.8}$$

where V_H, and d are the Hall voltage and the thickness of the sample, respectively. In addition, ρ can be determined from the Van der Pauw method[73] by measuring successively the resistance R_A and R_B between two contacts on the vertical and horizontal edges, corresponding to $R_A = V_{43}/I_{12}$ and $R_B = V_{14}/I_{23}$. Thus, ρ can be extract according to the relationship:

$$\exp\left(-\frac{\pi t R_A}{\rho}\right) + \exp\left(-\frac{\pi t R_B}{\rho}\right) = 1. \tag{3.9}$$

Finally, the mobility μ_H can be determined according to the relation $\mu_H = (q n_H \rho)^{-1}$.

3.6 Secondary Ion Mass Spectrometry (SIMS)

Secondary ion mass spectrometry (SIMS)[78] is a powerful technique used to analyze the amount of impurities in solid materials. Figure 3.9 shows a schematic overview of a magnetic sector SIMS instrument. A focused primary ion beam is used to sputter the surface of the sample. The charged atoms and molecules emerging from the sample are accelerated and focused into a "secondary" ion beam. This secondary ion beam is analyzed using a mass spectrometer. Thus, the instrument is able to record a mass spectrum of the sample, depth profile of impurities and lateral distribution of impurities. SIMS is a very sensitive technique able to measure impurities concentration in the part per billion range, which makes it very suitable to study impurities in semiconductors. Further, depth resolution as low as 2 nm can be achieved, which enables studies of very abrupt impurity depth profiles. However, SIMS is a destructive technique, which may be a drawback in certain cases.

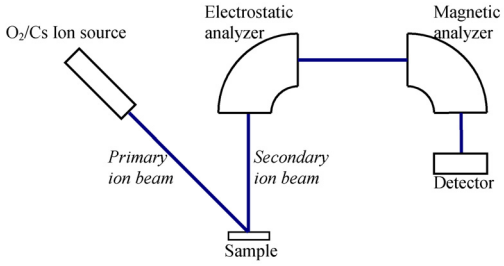

Figure 3.9: Schematic of the SIMS instrument.

In this thesis, a Cameca IMS-7f system equipped with oxygen and cesium primary ion sources has been used to give quantitative information on the impurities concentrations in both bulk and thin film ZnO. In addition, in the case of heterojunction ZnO/Si samples, depth profiles of impurities have been determined.

Chapter 4

Summary of results

The results obtained during the work of this thesis can be divided into two parts: the investigation of defects in bulk ZnO and the electric properties of ZnO/Si heterostructures, deposited by magnetron sputtering or atomic layer deposition (ALD). A summary of the results will be given in the following sections.

4.1 Bulk HT-ZnO

4.1.1 Sample preparation

$1 \times 1 \times 0.5\ cm^3$ hydrothermally grown ZnO wafers from SPC Goodwill have been used in this thesis to investigate bulk defects. As described in chapter 2, HT-ZnO is highly resistive, principally due to the presence of lithium in significant concentration which acts as compensating center. Therefore, the ZnO wafers were heat treated at high temperature to reduce the lithium concentration by about two orders of magnitude from the $\sim 10^{17}$ to $\sim 10^{15}\ cm^{-3}$.[17] After annealing, the surface roughness increased drastically and the samples were subsequently manually polished on both sides on a rotating disc with diamond slurry using different grain sizes from 6 to 0.25 μm. The polishing process removes a layer of 20-30 μm in thickness. During the annealing treatment lithium diffuses out of the sample; however, a fraction remains accumulated at the surface.[17] The polishing allows to remove the accumulated Li at the surface.

A post polishing etching process has been developed to remove the defects caused by the polishing. After polishing, the samples were dipped in a 2% hydrofluoric acid (HF) solution at room temperature for 2 min. This treatment removes gently around 200 nm of the top layer of ZnO, previously exposed to the polishing.

Schottky contacts were prepared on Zn-polar face using Palladium (Pd). The samples were first cleaned in acetone and isopropanol for 5 min each in a ultrasonic bath, followed by treatment in 40% hydrogen peroxide (H_2O_2) solution at boiling temperature for 1 min. This pretreatment is intended to improve the quality and the stability of the Schottky contacts. Finally, 100 nm thick circular Pd contacts were deposited using electron beam evaporation from a 99.999% pure Pd source through a molybdenum shadow mask at a base pressure of 10^{-6} mbar. The circular contacts had a diameter of 0.30, 0.50 and 0.80 mm. Silver paste was used as Ohmic contact on the back side (O-face).

4.1.2 Effect of the annealing condition on the electrical characteristics of ZnO

Several samples have been heat treated in different atmospheres. Table 4.1 summarizes the carrier concentrations obtained from C-V measurements for the different annealing conditions. In this thesis, 8 wafers have been used (labelled 1 to 8), each cut in 4 pieces (labelled a, b, c and d).

After annealing HT-ZnO samples under the same condition, e.g. 1400°C in Ar ambient during 1 hour, the carrier concentration was found to be different for each wafer and varied from 5×10^{16} to 3×10^{17} cm^{-3} (see Table 4.1). This indicates that the growth conditions may substantially influence the donor concentration, in accordance with results reported in the literature.[24] However, also depending on the annealing conditions, the carrier concentration can be influenced. For example, O-rich annealing leads to a reduction in the carrier concentration (samples 2-a, 4-a, 5-a and 7-a) compared to the other ambients. In contrast, the Zn-rich annealing results in an increase of the carrier concentration. Thus, even if the growth process is the most important factor for controlling the carrier concentration, a variation of the $[Zn]/[O_2]$ ratio during post-growth heat treatment results in a modification of the net carrier concentration.

Table 4.1: Summary of samples annealed in different conditions and their respective carrier concentrations, as determined from C-V measurements. The number corresponds to the wafer and the letter corresponds to the part of the wafer.

Annealing	Sample	Carrier concentration (cm^{-3})
as-grown	4-d	3×10^{17}
	8-a	1×10^{17}
1500°C, O_2, 1h	4-a	1×10^{17}
	5-b	5×10^{16}
1500°C, N_2, 1h	4-b	1×10^{17}
1400°C, O_2, 1h	1-a	5×10^{16}
	5-a	8×10^{16}
	6-a	9×10^{16}
	7-a	4×10^{16}
1400°C, N_2, 1h	1-b	9×10^{16}
	6-b	2×10^{17}
1400°C, Ar, 1h	1-c	7×10^{16}
	2-a	2×10^{17}
	6-c	1×10^{17}
	7-b	5×10^{16}
1400°C, N_2, 1h and	1-d	8×10^{16}
700°C, N_2/H_2, 2h	4-c	8×10^{16}
1100°C, Zn-rich, 30min	1-c	1×10^{17}
	2-a	3×10^{17}

As illustrated by Fig. 4.1, typical DLTS measurements carried out on HT-ZnO unveil 3 main defect levels in the 70-300K temperature range with energy positions and apparent capture cross sections summarized in table 4.2. Moreover, improvements made on the Pd contacts quality have allowed DLTS measurements at temperatures up to 600K, which enables investigation of defect levels close to the middle of the band gap. Thus, two additional defect levels have been observed in the 300-600K temperature range (see Fig. 4.1(c)), labelled E5 and E6. Their energy positions and apparent capture cross sections are summarized in table 4.2.

Table 4.2: Survey of the energy position and apparent capture cross section of defect levels observed in HT-ZnO by DLTS.

Defect	$E_c - E_t$ (eV)	σ_{na} (cm^2)
E2	0.19	6×10^{-17}
E3	0.30	2×10^{-15}
E4	0.54	1×10^{-13}
E5	1.00	8×10^{-14}
E6	1.20	4×10^{-15}

A control of the annealing conditions in various ambients allows to alter the concentration of intrinsic defect levels of ZnO and can provide information on their origin. Papers I and III summarize the effect of different annealing conditions on the concentration of the defect levels observed by DLTS.

In paper I, one HT-ZnO wafer was cut into 4 samples, labelled 1-a, 1-b, 1-c and 1-d. The samples 1-a, 1-b and 1-c were annealed at 1400°C for 1 hour in O_2, N_2 and Ar atmosphere, respectively. The sample 1-d was heat treated at 1400°C for 1 hour in N_2 and subsequently at 700°C for 2 hour in N_2/H_2 (90%/10%). The DLTS measurements performed in the 80-300K temperature range show 3 defect levels, E2, E3 and E4, and TAS measurements reveal a freeze out level with energy position of ∼30 meV below E_c. In addition, TSCAP measurements show two capacitances step which correspond of the thermal emission of E2 and E3 defect levels in the bulk of the depletion region. The annealing conditions have a pronounced influence on the concentration of the observed defect levels E2, E3 and E4. The treatment in O_2 atmosphere yields a reduction in E2 and E3 and an increase of E4, relative to the other annealing conditions. Therefore,

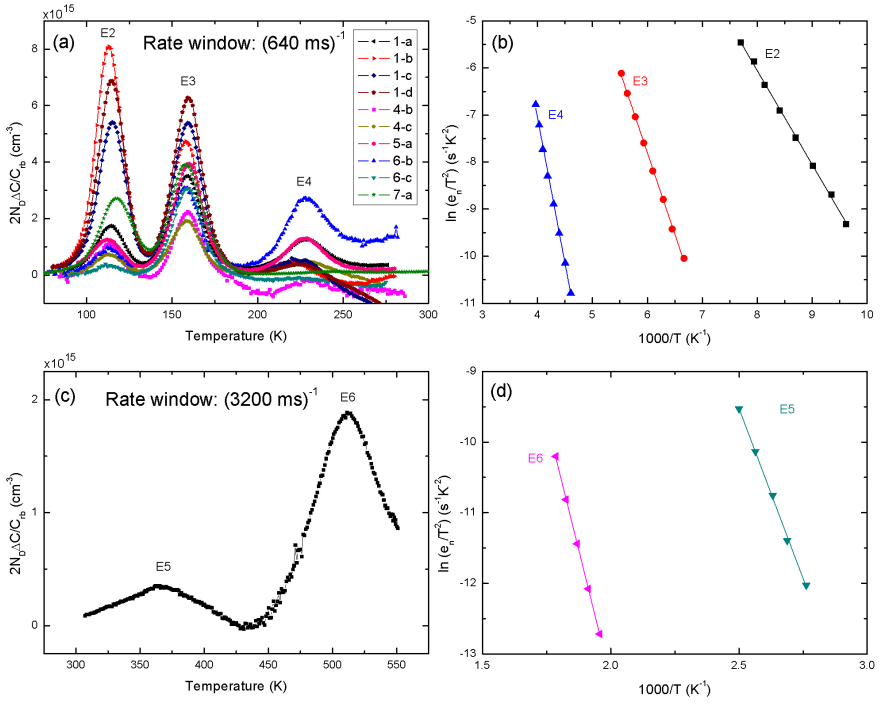

Figure 4.1: (a) Representative DLTS spectra of different samples investigated in this thesis showing the three defect levels E2, E3 and E4 and (b) their corresponding Arrhenius plots of the electron emission rate. (c) DLTS spectra made in the 300-600K temperature range showing two defect levels E5 and E6 and (d) their corresponding Arrhenius plots.

one may speculate that E2 and E3 arise from an oxygen deficient defects (V_O, Zn_O and Zn_i) and E4 from a zinc deficient defect (V_{Zn}, O_{Zn} and O_i). However, a comparison with another sample coming from wafer 2 treated under the same condition as 1-c, exhibits dramatically higher concentration of E2 and E3 than sample 1-c. So, the origin of the sample has a substantial influence on the defect concentrations and the role of impurities cannot be excluded.

In paper III, the samples, coming from the two wafers 1 and 2 used in the paper I and annealed in Ar atmosphere (1-c and 2-a), were additionally heat treated in O-rich condition at 1100°C for 1 hour and in Zn-rich at 1100°C for 30 min. DLTS measurements were carried out between the different annealing steps. After Ar annealing, the two samples (labelled samples A0 and B0 in the paper) present substantial difference in the concentration of E2 and E3. The two extra annealing steps in Zn-rich (samples A1 and B2) and O-rich (samples A2 and B1) conditions have a strong influence on E2 and E4. However, E3 is not influenced by the different annealing treatments at 1100°C, which indicates a high formation energy of E3, in agreement with the literature where a temperature higher than 1300°C is required to modify its concentration.[24] The treatment in Zn atmosphere removes E2 and yields an increase in E4 by a factor of ~ 4, relative to O_2 atmosphere. After the treatment in O_2 atmosphere, the opposite holds with the formation of E2 and removal of E4. Thus, one can speculate that E4 originates from a Zn-rich defect (V_O, Zn_i and Zn_O) and E2 from an O-rich defect (V_{Zn}, O_i and O_{Zn}). In addition, E4 was influenced in the same absolute manner for both samples, exhibiting almost identical concentration after the Zn-rich annealing (samples A1 and B2). This may indicate an intrinsic nature of E4 and by assuming that thermal equilibrium is reached, a formation energy of 1.9 eV of E4 has been determined. The E2 level exhibits a Poole-Frenkel effect which indicates that it arises from a donor-like defect. Moreover, after the O-rich annealing, the concentration of E2 varies by a factor $\sim$5 between the two samples (A2 and B1). This variation excludes a pure intrinsic nature and can imply that E2 arises from an impurity complex activated by O-rich heat treatment. A comparative study between DLTS and SIMS has been performed on samples with a large range of E2 concentrations but no direct correlation with any specific impurity element has been established.

At a first glance, the results obtained in paper I and paper III appear to be contradictory regarding the assignment of E2 and E4. However, the results in paper III are, indeed, more conclusive and less speculative than the ones in paper I. For instance, in paper I the variation in E4 concentration is about a factor of two between the different atmospheres used (O_2, N_2, Ar, N_2/H_2) while in paper III the enhancement is about a factor of 20 using Zn-rich atmosphere relative to O_2 atmosphere. Further, as already discussed preliminary in paper I E2 is impurity-related, in contrast to E4 which seems to be of intrinsic origin, and its concentration hinges not only on the annealing atmosphere but also on the sample history. The reversible variations in the E2 amplitude by more than a factor of 20 between consecutive treatments using Zn- and O-rich atmospheres for the same sample in paper III are considered as unambiguous while the variations by a factor of 4-5 between different samples in paper I and primarily attributed to variations in the impurity content.

4.1.3 Effect of polishing

As described in Section 2.3, ZnO is a soft material and processing may damage or introduce defects in the near surface region, e.g. after polishing. Thus, processing can influence the electrical properties of ZnO and may severely limit device performance. In paper II, the effect of polishing on the electrically active defects in ZnO has been investigated by C-V and DLTS measurements using Pd Schottky contacts deposited on the polished surface (Zn-face). It is shown that mechanical polishing forms defects in the near surface region that strongly compensate and/or passivate the dominant donors, which result in a depletion region extending deep into the bulk. Further, two pronounced defect levels are observed with energy positions around $\sim$1.0 eV and $\sim$1.2 eV below E_c (see Fig. 4.1(c)). A post-polishing etching in diluted hydrofluoric acid removes the top layer exposed to the polishing process, and then, the carrier concentration has a constant profile and the depletion region is close to the interface. In addition, the two pronounced defects are substantially reduced, by a factor of $\sim$10. These levels are tentatively identified as vacancy related defects based on previously reported optical transitions and PAS data by other authors.[51, 61, 79]

4.1.4 Ion implantation

An ion implantation study has been conducted, using hydrothermally n-type ZnO samples purchased from Tokyo Denpa, and without annealing and subsequent polishing prior to contact formation (Paper IV). Before implantation, the samples have uniform carrier concentration of $N_D = 1 \times 10^{15}\, cm^{-3}$, and DLTS measurement reveals only the E3 level. The polishing-induced levels E5 and E6, reported in paper II, are not observed in the as-grown samples. The samples were then implanted with 3 MeV and 6 MeV Zn^+ ions at room temperature using doses from 1×10^8 to $2 \times 10^{10}\, cm^{-2}$. C-V measurements show charge carrier compensation by deep acceptor-like defects along the implantation depth profile. In addition, DLTS measurements reveal four implantation-related defect levels with energy positions of 0.57, 0.89, 1.06 and 1.2 eV below E_c. Interestingly, defect levels similar to E5 and E6 appear after the ion implantation and show a strong dose dependence. This illustrates the importance of the levels studied in paper II, and supports an intrinsic origin of E5 and E6.

4.2 ZnO/Si heterostructure

The electronic properties of ZnO/Si heterojunctions have been investigated. Thin films of ZnO were deposited on Si wafers by magnetron sputtering or ALD. ZnO/Si contacts were formed, by lithography. However, for practical reasons, and to improve the contact quality between the needle of the electrical probe and the ZnO layer, a second process has been developed by depositing circular Ni Ohmic contacts on the ZnO layer through a shadow mask using e-beam evaporation. These Ni contacts are also used as mask when etching the ZnO layer to form a Ni/ZnO/Si structure. After the contact formation, I-V, C-V and DLTS measurements have been performed to investigate the electrical properties and the defects close to the interface of ZnO/Si heterostructures. Paper V shows the results obtained for the heterojunction n-ZnO(Al)/p-Si prepared by dc magnetron sputtering. Papers VI and VII summarize the results obtained on ZnO/Si prepared by ALD. Finally, a comparison between ZnO/Si structures prepared by ALD and RF magnetron sputtering is given in section 4.2.3.

4.2.1 DC Magnetron Sputtering

In paper V, Al-doped ZnO has been deposited at room temperature on p-type Si and subsequently annealed in the 100-400°C temperature range. I-V, C-V and DLTS measurements were performed to investigate the electronic properties of the heterojunctions. A diode like junction is revealed with a rectification up to 4 orders of magnitude and high ideality factor of ~ 5, indicating a poor quality of the junction. For samples annealed below 150°C, a reduction of the hole concentration occurs close to the interface, suggesting compensation of the boron dopant by donor type defects or passivation by formation of boron-hydrogen pairs during the sputtering process. After annealing at 150-200°C, the compensating/passivating defects disappear and the carrier concentration recovers with a constant profile. The DLTS measurements reveal defect levels located near to the ZnO(Al)/p-Si interface; i.e., two hole traps labelled H(0.38) and H(0.43) with energy positions and apparent capture cross sections corresponding to $E_v + 0.38\,eV$ and $5 \times 10^{-14}\,cm^2$, and $E_v + 0.43\,eV$ and $1 \times 10^{-17}\,cm^2$, respectively. H(0.38) is present in all samples irrespective of the annealing treatment while H(0.43) appears after heat treatment above 250°C.

4.2.2 Atomic Layer deposition

In paper VI, ZnO/n-Si and ZnO/p-Si heterostructures have been studied where the ZnO thin films were deposited by ALD at 175°C and post-heat treated in the 200-500°C temperature range. The structural and electrical properties of the junctions have been investigated by X-ray diffraction (XRD), I-V, and DLTS techniques. The XRD results of the as-deposited sample show that the ZnO layer is polycrystalline and randomly oriented with two prominent peaks occurring from the (100) and (002) directions. The post-deposition heat treatment at 400°C results in an improvement of the crystal structure with a preferred orientation along the c-axis. DLTS measurements show two dominant electron traps at the interface of the ZnO/n-Si junction, while no electrically active defects were detected at the interface of ZnO/p-Si. The two electron traps, labelled E(0.07) and E(0.15), have energy position and apparent capture cross section corresponding to $E_c - 0.07\,eV$ and $1 \times 10^{-23}\,cm^2$, and $E_c - 0.15\,eV$ and

$1 \times 10^{-22}\, cm^2$, respectively. E(0.07) is annealed out at 500°C, while E(0.15) grows with heat treatment at 500°C.

In paper VII, a study of the barrier heights and the current transport mechanism in the ZnO/n-Si and ZnO/p-Si heterostructures prepared by ALD has been carried out. The structure of the junction has been investigated by cross section Transmission Electron Microscopy (TEM) and reveals a random orientation of the ZnO grains in accordance with the XRD results obtained in paper VI. At the interface, a thin layer of SiO_x ($x \leq 2$) is observed with an homogeneous thickness of ~ 0.4 nm. Hall measurement indicates a degenerate ZnO layer with carrier concentration of $\sim 10^{19}\, cm^{-3}$ and mobility of $\sim 20\, cm^2 V^{-1} s^{-1}$. The n-type doping is mainly assigned to hydrogen and/or hydrogen related complexes, which are present in high concentration ($\sim 10^{20} - 10^{21}\, cm^{-3}$) in the ZnO films. Thus, the ZnO/Si structures may be approximated as a metal-semiconductor contact. In addition, the good interface allows detailed and accurate determination of the work function, Φ_{ZnO}. Hence, I-V and C-V have been performed in the 50-300K temperature range in order to determine the barrier heights of the junctions through the thermal emission theory. Both ZnO/n-Si and ZnO/p-Si show rectifying contacts with barrier heights of 0.61 eV and 0.52 eV, respectively. The barriers obtained from C-V are found to be slightly higher than those from I-V but remain of the same order. In addition, the sum of the barrier heights is found to be close to the band gap of Si and these consistent results yield an estimate of the work function of ZnO as $\Phi_{ZnO} = 4.65$ eV.

The effects of post-annealing treatments on the electrical properties of the ZnO layer have been studied by four point probe and Hall effect measurements. The impurity content in the ZnO films has been investigated by SIMS. For as-deposited samples, the main impurities are hydrogen ($\sim 5 \times 10^{20}\, cm^{-3}$) and carbon ($\sim 2 \times 10^{19}\, cm^{-3}$) coming from the precursors used during the ALD growth. The n-type doping is, most likely, attributed to hydrogen and/or hydrogen related complexes acting as shallow donors. In addition, hydrogen may also passivate the acceptor defects. After annealing, the ZnO films become highly resistive ($\rho \sim 800\ \Omega.cm$ after 250°C), while the hydrogen content remains constant. Hydrogen is expected to be mobile even at low temperature,

so one can speculate that the annealing treatment modifies the hydrogen configuration, effectively passivating the donor activity.

4.2.3 Comparison of ZnO/Si junctions prepared by ALD and RF Magnetron Sputtering

A preliminary investigation has been performed to compare ZnO/Si heterostructures in detail prepared by ALD and RF magnetron sputtering techniques. Hence, ZnO and Al-doped ZnO thin films have been deposited on Si by ALD and RF magnetron sputtering, respectively. The structure and the interface of the heterostructures have been investigated by TEM and DLTS. Cross section TEM images of the sputtered samples show a structure with a preferential growth along the c-axis, while the ALD samples have grains with random orientation. The interface of the junctions reveals a SiO_x layer with a thickness of ∼2 nm and ∼0.4 nm for the sputtered and ALD samples, respectively. DLTS measurements of the interface region unveil at least five defect levels in the sputtered samples and only one in the ALD samples (see Fig. 4.2). These results demonstrate clearly that ALD is a soft deposition technique which induces less defects at the interface, while sputtering, due to energetic ions in the plasma, tends to induce a multitude of different defects.

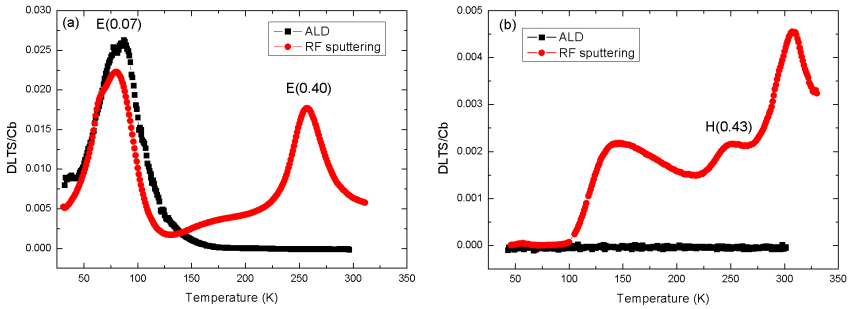

Figure 4.2: DLTS spectra of the interface region of (a) ZnO/n-Si and (b) ZnO/p-Si heterostructures prepared by ALD and RF magnetron sputtering.

Chapter 5

Conclusions and suggestions for further work

The work in this thesis is devoted to the investigation of the electrical properties of hydrothermally grown ZnO and ZnO/Si heterojunctions. Especially, the characterization of defect levels in the band gap of ZnO and at the interface of ZnO/Si heterostructures has been achieved. The obtained results will allow to contribute to the improvement of the properties of ZnO and, thus, increase its competitiveness in optoelectronic applications.

The first part of the thesis is focused on hydrothermally grown ZnO, described in Papers I-IV, and is mainly devoted to the investigation of electrically active defects by DLTS and TAS through Pd Schottky contacts. In particular, the effect of the different annealing conditions on the defect levels has been investigated in order to identify the origin of the defects. Thus, some defect levels show strong dependence on the annealing conditions. For example, E2 and E4 appear as O-rich and Zn-rich defects, respectively. Moreover, the improvement made on the Pd Schottky contacts has allowed us to explore deep states in the band gap of ZnO by using DLTS in the temperature range up to 600K. In the 300-600K interval, two new defect levels have been observed with energy position in the range $\sim$1.0-1.2 eV below E_c. These levels occur both after mechanical polishing and Zn ion implantation, which may suggest an intrinsic nature of E5 and E6. In general, the results obtained in this thesis have provided additional and useful information on several of these defect levels (E2, E3, E4, E5 and E6) as summarized in

table 2.4.

The second part of the thesis is devoted to electrical characterization of ZnO/Si heterostructures prepared by DC magnetron sputtering and ALD, described in papers V-VII. Degenerated ZnO films have been used as transparent contacts on Si. The electronic and interface properties of such heterostructures have been investigated by I-V, C-V and DLTS. The junctions show rectifying behavior on both n-type and p-type Si and several defect levels have been observed close to the interface. Moreover, the barrier heights of the ZnO/Si heterostructures prepared by ALD have been investigated by I-V and C-V versus temperature and consistent results are obtained to estimate the work function of ZnO as $\Phi_{ZnO} = 4.65$ eV. Finally, preliminary work has been done to compare ALD and RF magnetron sputtering and the results demonstrate that ALD is a soft deposition technique which induces less interfacial defects than sputtering.

The results in this thesis have clarified some properties of bulk ZnO, but several issues need to be pursued further. For example, it is necessary to improve the Schottky contacts in order to increase their stability and reproducibility. Hence, the development of Schottky contacts with other metals will be an important improvement for the characterization of ZnO and represents a future challenge. The annealing conditions in Zn- and O-rich ambients have strong effect on several defect levels and give preliminary suggestions on the origin of the defects. Therefore, more efforts should be devoted along this direction in order to confirm the origin of the defects, e.g., performing similar annealing treatment on samples grown with other techniques than HT may give more information on the origin of the defects (intrinsic or impurity related defect). Accordingly, combining the obtained results in this thesis with other techniques, such as photoluminescence, cathodoluminescence, infra-red spectroscopy and positron annihilation spectroscopy could be useful to determine the origin of the defects and to find some possibilities to limit (control) their concentrations in ZnO.

Concerning ZnO/Si heterostructures, ALD is a promising technique to deposit ZnO with low interfacial defects. However, further work has to be pursued on several points. The origin of the n-type doping of the ZnO films has to be addressed carefully. In particular, the role of hydrogen for the n-type conduction and its behavior after annealing must be investigated. Fourier transform infrared (FTIR) spectroscopy could be useful

to determine the hydrogen configuration in the ZnO films. Moreover, the control of the carrier concentration and mobility needs to be improved, especially for highly doped films. Further work must also be devoted to compare RF magnetron sputtering and ALD and, as a next step, the photovoltaic behavior of the heterostructures should be investigated.

References

[1] C. Jagadish and S. J. Pearton, *Zinc Oxide Bulk, Thin Films and Nanostructures* (Elsevier, Oxford, 2006).

[2] K. Ellmer, A. Klein, and B. Rech, *Transparent Conductive Zinc Oxide: basics and applications in thin film solar cells* (Springer, 2008).

[3] V. A. Coleman, *Processing and characterization of ZnO for device applications.*, Ph.D. thesis, The Australian National University (2006).

[4] T. Coutts, T. Mason, J. Perkins, and D. Ginley, Meeting of the Electrochemical Society (1999).

[5] T. Minami, Semicond. Sci. Technol. **20**, S35 (2005).

[6] M. Trunk, V. Venkatachalapathy, A. Galeckas, and A. Y. Kuznetsov, Appl. Phys. Lett. **97**, 211901 (2010).

[7] V. Venkatachalapathy, A. Galeckas, R. Sellappan, D. Chakarov, and A. Y. Kuznetsov, J. Cryst. Growth **315**, 301 (2011).

[8] A. M. Gas'kov and M. N. Rumyantseva, Russ. J. Appl. Chem. **74**, 440 (2001).

[9] S. J. Pearton, D. P. Norton, K. Ip, Y. W. Heo, and T. Steiner, Prog. Mater. Sci. **50**, 293 (2005).

[10] S. J. Pearton, D. P. Norton, Y. W. Heo, L. C. Tien, M. P. Ivill, Y. Li, B. S. Kang, F. Ren, J. Kelly, and A. F. Hebard, J. Electron. Mater. **35**, 862 (2006).

[11] R. Schifano, *Schottky contacts and electrical characterization of n-type hydrothermally grown ZnO*, Ph.D. thesis, Univerity of Oslo, Norway (2009).

[12] L. J. Brillson and Y. Lu, J. Appl. Phys. **109**, 121301 (2011).

[13] E. Rhoderick and R. Williams, *Metal-Semiconductor contacts*, edited by Oxford (Oxford university press, 1988).

[14] W. Shockley and W. T. Read, Phys. Rev. **87**, 835 (1952).

[15] R. N. Hall, Phys. Rev. **87**, 387 (1952).

[16] J. Frenkel, Phys. Rev. **54**, 647 (1938).

[17] E. V. Monakhov, A. Y. Kuznetsov, and B. G. Svensson, J. Phys. D: Appl. Phys. **42**, 153001 (2009).

[18] A. Janotti and C. G. Van de Walle, Appl. Phys. Lett. **87**, 122102 (2005).

[19] A. Janotti and C. G. Van de Walle, Phys. rev. B **76**, 165202 (2007).

[20] C. G. Van de Walle, Physica B **308-310**, 899 (2001).

[21] M. D. McCluskey, S. J. Jokela, K. K. Zhuravlev, P. J. Simpson, and K. G. Lynn, Appl. Phys. Lett. **81**, 3807 (2002).

[22] M. H. Weber and K. G. Lynn, J. Phys.: Conf. Ser. **262**, 012063 (2011).

[23] M. D. McCluskey and S. J. Jokela, Physica B **401-402**, 355 (2007).

[24] L. Vines, E. V. Monakhov, and B. G. Svensson, Physica B **404**, 4386 (2009).

[25] K. Ellmer, J. Phys. D: Appl. Phys. **33**, R17 (2000).

[26] H. Agura, A. Suzuki, T. Matsushita, T. Aoki, and M. Okuda, Thin solid films **445**, 263 (2003).

[27] U. Özgür, Y. I. Alivov, C. Liu, A. Teke, M. A. Reshchikov, S. Doğan, V. Avrutin, S.-J. Cho, and H. Morkoç, J. Appl. Phys. **98**, 041301 (2005).

[28] A. Janotti and C. G. Van de Walle, Rep. Prog. Phys. **72**, 126501 (2009).

[29] K. Minegishi, Y. Koiwai, Y. Kikuchi, K. Yano, M. Kasuga, and A. Shimizu, Jpn. J. Appl. Phys. **36**, L1453 (1997).

[30] D. C. Look, Semicond. Sci. Technol. **20**, S55 (2005).

[31] R. Schifano, E. V. Monakhov, U. Grossner, and B. G. Svensson, Appl. Phys. Lett. **91**, 193507 (2007).

[32] W. Mtangi, F. D. Auret, C. Nyamhere, P. J. Janse van Rensburg, A. Chawanda, M. Diale, J. M. Nel, and W. E. Meyer, Physica B **404**, 4402 (2009).

[33] M. W. Allen, M. M. Alkaisi, and S. M. Durbin, Appl. Phys. Lett. **89**, 103520 (2006).

[34] H. von Wenckstern, G. Biehne, R. A. Rahman, H. Hochmuth, M. Lorenz, and M. Grundmann, Appl. Phys. Lett. **88**, 092102 (2006).

[35] J. Nause and B. Nemeth, Semicond. Sci. Technol. **20**, S45 (2005).

[36] D. C. Look, D. C. Reynolds, J. R. Sizelove, R. L. Jones, C. W. Litton, G. Cantwell, and W. C. Harsch, Solid State Commun. **105**, 399 (1998).

[37] K. Maeda, M. Sato, I. Niikura, and T. Fukuda, Semicond. Sci. Technol. **20**, S49 (2005).

[38] L. Vines, E. V. Monakhov, R. Schifano, W. Mtangi, F. D. Auret, and B. G. Svensson, J. Appl. Phys. **107**, 103707 (2010).

[39] A. Suzuki, T. Matsushita, N. Wada, Y. Sakamoto, and M. Okuda, Jpn. J. Appl. Phys. **35**, L56 (1996).

[40] A. V. Singh, R. M. Mehra, N. Buthrath, A. Wakahara, and A. Yoshida, J. Appl. Phys. **90**, 5661 (2001).

[41] R. Triboulet and J. Perrière, Prog. Cryst. Growth Charact. Mater. **47**, 65 (2005).

[42] S. J. Lim, S. Kwon, and H. Kim, Thin solid films **516**, 1523 (2008).

[43] A. Yamada, B. Sang, and M. Konagai, Appl. Surf. Sci. **112**, 216 (1997).

[44] Z. B. Ayadi, L. E. Mir, K. Djessas, and S. Alaya, Mater. Sci. Eng. C **28**, 613 (2008).

[45] N. Huby, S. Ferrari, E. Guziewicz, M. Godlewski, and V. Osinniy, Appl. Phys. Lett. **92**, 023502 (2008).

[46] E. Przeździecka, Ł. Wachnicki, W. Paszkowicz, E. Łusakowska, T. Krajewski, G. Łuka, E. Guziewicz, and M. Godlewski, Semicond. Sci. Technol. **24**, 105014 (2009).

[47] E. M. Kaidashev, M. Lorenz, H. von Wenckstern, A. Rahm, H.-C. Semmelhack, K.-H. Han, G. Benndorf, C. Bundesmann, H. Hochmuth, and M. Grundmann, Appl. Phys. Lett. **82**, 3901 (2003).

[48] K. Miyamoto, M. Sano, H. Kato, and T. Yao, J. Cryst. Growth **265**, 34 (2004).

[49] D. W. Hamby, D. A. Lucca, and M. J. Klopfstein, J. Appl. Phys. **97**, 043504 (2005).

[50] T. M. Børseth, P. Klason, Q. X. Zhao, M. Willander, B. G. Svensson, and A. Y. Kuznetsov, Appl. Phys. Lett. **89**, 262112 (2006).

[51] J. Mass, M. Avella, J. Jiménez, A. Rodríguez, T. Rodríguez, M. Callahan, D. Bliss, and B. Wang, J. Cryst. Growth **310**, 1000 (2008).

[52] Y. Dong, F. Tuomisto, B. G. Svensson, A. Y. Kuznetsov, and L. J. Brillson, Phys. Rev. B **81**, 081201 (2010).

[53] J. C. Simpson and J. F. Cordaro, J. Appl. Phys. **63**, 1781 (1988).

[54] G. Brauer, W. Anwand, W. Skorupa, J. Kuriplach, O. Melikhova, C. Moisson, H. von Wenckstern, H. Schmidt, M. Lorenz, and M. Grundmann, Phys. rev. B **74**, 045208 (2006).

[55] Y. Jiang, N. C. Giles, and L. E. Halliburton, J. Appl. Phys. **101**, 093706 (2007).

[56] F. D. Auret, J. M. Nel, M. Hayes, L. Wu, W. Wesch, and E. Wendler, Superlattices and Microst. **39**, 17 (2006).

[57] H. von Wenckstern, H. Schmidt, M. Grundmann, M. W. Allen, P. Miller, R. J. Reeves, and S. M. Durbin, Appl. Phys. Lett. **91**, 022913 (2007).

[58] L. Scheffler, V. l. Kolkovsky, E. V. Lavrov, and J. Weber, J. Phys.: Condens. Matter **23**, 334208 (2011).

[59] L. Vines, J. Wong-Leung, C. Jagadish, E. V. Monakhov, and B. G. Svensson, Physica B , article in press (2011).

[60] J. E. Bradby, S. O. Kucheyev, J. S. Williams, C. Jagadish, M. V. Swain, P. Munroe, and M. R. Phillips, Appl. Phys. Lett. **80**, 4537 (2002).

[61] F. A. Selim, M. H. Weber, D. Solodovnikov, and K. G. Lynn, Phys. Rev. Lett. **99**, 085502 (2007).

[62] R. Schifano, E. V. Monakhov, L. Vines, B. G. Svensson, W. Mtangi, and F. D. Auret, J. Appl. Phys. **106**, 043706 (2009).

[63] R. Schifano, E. V. Monakhov, B. G. Svensson, W. Mtangi, P. Janse van Rensburg, and F. D. Auret, Physica B **404**, 4344 (2009).

[64] M. Hayes, F. D. Auret, P. J. Janse van Rensburg, J. M. Nel, W. Wesch, and E. Wendler, Nucl. Instrum. Meth. B **257**, 311 (2007).

[65] U. Grossner, S. Gabrielsen, T. M. Børseth, J. Grillenberger, A. Y. Kuznetsov, and B. G. Svensson, Appl. Phys. Lett. **85**, 2259 (2004).

[66] F. D. Auret, S. A. Goodman, M. J. Legodi, W. E. Meyer, and D. C. Look, Appl. Phys. Lett. **80**, 1340 (2002).

[67] T. Frank, G. Pensl, R. Tena-Zaera, J. Zúniga-Pérez, C. Martínez-Tomás, V. Munoz-Sanjosé, T. Ohshima, H. Itoh, D. Hofmann, D. Pfisterer, J. Sann, and B. Meyer, Appl. Phys. A **88**, 141 (2007).

[68] O. Lopatiuk, L. Chernyak, A. Osinsky, and J. Q. Xie, Appl. Phys. Lett. **87**, 214110 (2005).

[69] K. Kuriyama, M. Ooi, K. Matsumoto, and K. Kushida, Appl. Phys. Lett. **89**, 242113 (2006).

[70] Z.-Q. Fang, B. Claflin, D. C. Look, and G. C. Farlow, J. Appl. Phys. **101**, 086106 (2007).

[71] F. D. Auret, S. A. Goodman, M. Hayes, M. J. Legodi, H. A. van Laarhoven, and D. C. Look, Appl. Phys. Lett. **79**, 3074 (2001).

[72] J. H. Werner and H. H. Güttler, J. Appl. Phys. **69**, 1522 (1991).

[73] P. Blood and J. Orton, *The Electrical Characterization of Semiconductors: Majority Carriers and Electron States.* (Academic Press, 1992).

[74] D. V. Lang, J. Appl. Phys. **45**, 3023 (1974).

[75] D. L. Losee, J. Appl. Phys. **46**, 2204 (1975).

[76] J. L. Pautrat, B. Katircioglu, N. Magnea, D. Bensahel, J. C. Pfister, and L. Revoil, Solid-St. Electron. **23**, 1159 (1980).

[77] C. T. Sah, W. W. Chan, H. S. Fu, and J. W. Walker, Appl. Phys. Lett. **20**, 193 (1972).

[78] K. M. Johansen, *Group one impurities in single crystalline Zinc Oxide*, Ph.D. thesis, Univerity of Oslo, Norway (2011).

[79] D. A. Lucca, D. W. Hamby, M. J. Klopfstein, and G. Cantwell, Physica Status Solidi B **229**, 845 (2002).

Paper I

Electrical Characterization of Hydrothermally Grown ZnO Annealed in Different Atmospheres.

V. Quemener, L. Vines, E.V. Monakhov and B.G. Svensson.

Int. J. Appl. Ceram. Technol., 8 [5] (2011) 1017-1022

Paper II

Electronic properties of vacancy related defects in ZnO induced by mechanical polishing.

V. Quemener, L. Vines, E.V. Monakhov and B.G. Svensson.

Appl. Phys. Lett. 99 (2011) 112112

Electronic properties of vacancy related defects in ZnO induced by mechanical polishing

V. Quemener,[a] L. Vines, E. V. Monakhov, and B. G. Svensson
University of Oslo, Department of Physics/Center for Materials Science and Nanotechnology, P.O. Box 1048 Blindern, N-0316 Oslo, Norway

(Received 1 July 2011; accepted 24 August 2011; published online 15 September 2011)

Electronic properties of defects induced by mechanical polishing in hydrothermally grown n-type ZnO have been investigated by capacitance versus voltage measurements and deep level transient spectroscopy (DLTS). The DLTS measurements have been performed in the temperature range 80-600 K enabling exploration of deep-level states in the vicinity of the middle of the energy bandgap. The results show that mechanical polishing forms defects in the near surface region which strongly compensate and/or passivate the dominant shallow donors. Two pronounced polishing-induced defects are revealed with energy level positions around 1.0 eV and 1.2 eV below the conduction band edge. These levels are assigned to vacancy-related defect centers and substantially reduced in strength by post-polishing etching in diluted hydrofluoric acid. © *2011 American Institute of Physics*. [doi:10.1063/1.3638470]

Zinc oxide[1] (ZnO) is a wide band gap semiconductor (Eg = 3.37 eV at room temperature) having a high potential for photovoltaic and light emitting devices. However, residual impurities and intrinsic defects can drastically affect the electrical characteristics of the material. Further, semiconductor device manufacture inevitably involves mechanical processes, such as polishing. Given that ZnO is a relatively "soft" material (hardness of ~5 GPa),[2] polishing-induced damage may severely limit potential device applications. Several authors have investigated the effects of polishing on the optical and structural properties of ZnO.[3–9] In particular, photoluminescence (PL), ion channeling, and cathodoluminescence have been employed showing that the mechanical polishing gives rise to subsurface damage which decreases luminescence efficiency[3,9] and results in several luminescence peaks related to intrinsic defects such as the zinc vacancy (V_{Zn}) and the zinc interstitial (Zn_i).[5,6] Most recently, the effect of polishing has also been investigated by positron annihilation spectroscopy (PAS) with the evidence of formation of open volume defects in the near surface region.[8] Despite these efforts, information about the electronic properties of polishing-induced defects in ZnO is scarce in the literature,[10] and one possible cause is the difficulty in achieving Schottky contacts of sufficient quality.

Recent works, however, have considerably improved the quality of Schottky contacts,[11–13] enabling investigations of the effect of mechanical polishing by spectroscopic electrical techniques. In particular, the improved Schottky contacts allow deep level transient spectroscopy (DLTS) measurements at sufficiently high temperatures to monitor deep states located close to the middle of the bandgap.

In this study, the influence of polishing on the electrically active defects in n-type ZnO has been investigated by capacitance versus voltage (C-V) and DLTS measurements. The DLTS studies were performed in the 80-600 K temperature range, which is a substantial progress in the study of deep-level defects in ZnO by junction spectroscopic techniques. The results unveil compensation/passivation of shallow donors and two pronounced deep levels having a strong dependence on the polishing process. Thus, mechanical polishing could be used as a possible way to controllably introduce intrinsic defects.

Samples were cut from a hydrothermally grown n-type ZnO (HT-ZnO) wafer with orientation perpendicular to the c-axis ([0001] direction) and annealed during 1 h at 1400°C in flowing oxygen. This annealing is known to reduce the Li content in HT-ZnO by about two orders of magnitude from the 10^{17} cm^{-3} to the 10^{15} cm^{-3} range.[14,15] After the heat treatment, the samples were mechanically polished on both sides on a rotating disc with diamond slurry using different grain sizes from 6 μm to 0.25 μm. The polishing process removes a layer with a total thickness of about 20-30 μm on each side.

After the polishing, Schottky contacts were prepared on the (0001) Zn-face using palladium (Pd). The samples were first cleaned in acetone and isopropanol in an ultrasonic bath for 5 min each. Then, the samples were dipped in a 40% hydrogen peroxide (H_2O_2) solution at boiling temperature for 1 min. Finally, 100 nm thick circular Pd contacts were deposited using electron beam evaporation from a 99.999% pure Pd source through a molybdenum shadow mask at a base pressure of 10^{-6} mbar. Silver paste was used as Ohmic contact on the back side (O-face). After a first set of measurements on one sample, labelled A1, the contacts were removed by a gentle polishing using diamond slurry (particles size of 0.25 μm) on a rotating disc. The A1 sample was then etched in a 2% hydrofluoric acid (HF) solution at room temperature (yielding an etch rate of ~2 nm/s, as determined using a DEKTAK stylus profilometer) for 2 min in order to remove the top layer exposed to the polishing process. Finally, new Schottky contacts were deposited on the Zn-face under the same conditions as previously described, and the sample was re-labelled as A2.

The C-V characteristics were recorded in dark at room temperature using a 1 MHz capacitance meter (HP 4280A).

[a]Electronic mail: vincent.quemener@smn.uio.no.

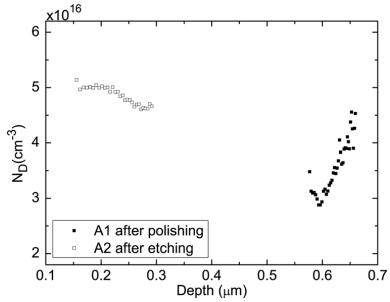

FIG. 1. Carrier concentration profiles determined by C-V measurements with a probe frequency of 1 MHz after polishing (sample A1) and after subsequent etching in 2% HF solution (sample A2).

The DLTS measurements were performed in the temperature range 80-600 K with a reverse bias voltage of −3 V and a pulse voltage of +3 V using a refined version of a setup described in Ref. 16. The DLTS signal was extracted applying a lock-in weighting function with different rate windows in the range $(20\ \text{ms})^{-1}$ to $(3200\ \text{ms})^{-1}$.

Figure 1 shows the net donor concentration profile after polishing (A1) and after etching in the HF solution (A2). The polishing influences strongly the carrier concentration profile; for A1, the depletion region extends deep into the bulk compared to A2, and the carrier concentration is increasing with depth ($N_D \approx 3 - 4 \times 10^{16}\ \text{cm}^{-3}$). This suggests that the dominant donors are passivated and/or compensated by defects present close to the surface. For A2, the carrier concentration has a uniform profile with $N_D \approx 5 \times 10^{16}\ \text{cm}^{-3}$ and the depletion region is close to the junction interface. In addition, the built-in voltage is reduced to ∼1 V, in close agreement with that predicted by the Schottky-Mott model for an ideal Pd/ZnO Schottky contact.[17] This confirms that the etching removes the surface layer damaged by polishing and the "ordinary" depletion region is recovered.

Figure 2 shows the DLTS spectra for the samples A1 and A2 using rate windows of $(640\ \text{ms}^{-1})$ and $(3200\ \text{ms}^{-1})$ in the 80-300 K and 300-600 K temperature intervals, respectively. The utilization of these two different windows

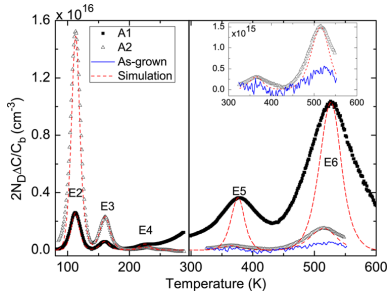

FIG. 2. (Color online) Measured (symbols) and fitted (dash line) DLTS spectra from samples A1, A2 and an as-grown sample not subjected to polishing/etching (solid line), using rate windows of $(640\ \text{ms}^{-1})$ and $(3200\ \text{ms}^{-1})$ in the temperature range of 80 K-300 K and 300 K-600 K, respectively. The inset shows a magnification of the DLTS spectra of the A2 and as-grown samples.

enables investigations of a wide range of electron emission rates while scanning over a limited temperature interval; especially, the $(3200\ \text{ms})^{-1}$ window facilitates detection of levels located close to the midgap using sample temperatures below 600 K. In the 80-300 K temperature range, three defect levels are observed, labelled E2, E3, and E4 with energy positions and apparent capture cross sections corresponding to $E_c - 0.18$ eV and $5 \times 10^{-17}\ \text{cm}^2$, $E_c - 0.30$ eV and $1 \times 10^{-15}\ \text{cm}^2$, and $E_c - 0.54$ eV and $1 \times 10^{-13}\ \text{cm}^2$, respectively ($E_c$ denotes the conduction band edge). These defects have previously been reported in the literature,[15,18,19] but their identities are still unclear. At elevated temperatures, two levels occur with peak maxima at ∼380 K and ∼500-540 K, labelled E5 and E6, respectively, and their intensities are enhanced by a factor of ∼25 relative to those found in as-grown samples not subjected to polishing. The signatures of E5 and E6, deduced from sample A2, are summarized in Table I.

The etching treatment, where a layer thickness up to 200 nm is removed from the surface, influences strongly the peak intensities with a reduction in E5 and E6 by a factor of ∼10 and in an increase in E2 and E3 by a factor of ∼5. The effect on E2 and E3 may be due to the different regions probed in samples A1 and A2 (see Fig. 1) and/or that compensating/passivating defects introduced by the polishing suppress the full amplitude of E2 and E3. Further work is needed to resolve this issue and in the following, we will focus on E5 and E6 levels.

By comparing the measured and simulated spectra for sample A1, the signatures of E5 and E6 are found to be about two times wider than a single DLTS peak simulated for a uniformly distributed and isolated point defect. These broad features of E5 and E6 indicate the presence of several different (extended) defects with overlapping levels or highly damaged regions with a high local concentration of defects. In the latter case, the defects can be distorted by surrounding local strain and are not to be considered as isolated point defects (as assumed in the simulations). In addition, after polishing, the measured apparent electron capture cross section, σ_{na}, of both E5 and E6 are unrealistically high ($\sigma_{na} \sim 10^{-8} - 10^{-12}\ \text{cm}^2$), further strengthening the indication of overlapping defects or localized damaged regions. For sample A2, the simulations agree rather closely with the measured E5 and E6 peaks and σ_{na} assumes more realistic values for deep-level point defects.

The samples A1 and A2 are physically the same specimen, and thus, the results in Figs. 1 and 2 show conclusively that the post-polishing etching in HF restores the concentration of shallow donors in the near surface region and reduces the concentration of E5 and E6 by a factor of ∼10, i.e., their intensities are almost comparable to those in the as-grown

TABLE I. Survey of the energy position and apparent capture cross section for E5 and E6 after etching (sample A2). The values are deduced from Arrhenius plots of the electron emission rates.

Sample	Defect	E_c-E_t (eV)	σ_{na} (cm^2)
A2 (after etching)	E5	1.0	8×10^{-14}
	E6	1.2	4×10^{-15}

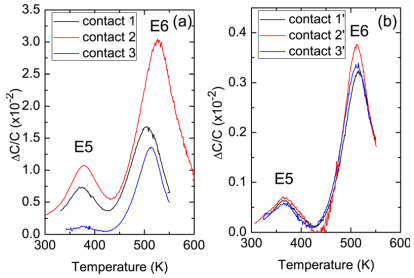

FIG. 3. (Color online) DLTS spectra of sample A1 (a) and sample A2 (b) for different contacts, measured in consecutive order on the same sample.

sample (Fig. 2 inset). In this context, it should be pointed out that the carrier concentration profile in sample A2 extends ~400 nm closer to the surface compared to that in sample A1 despite that a layer thickness of only ~200 nm was removed by the etching. Hence, the polishing-induced defects are not anticipated to be fully removed in sample A2 and other effects caused by in-diffusion of defects and impurities, like H from the HF etching, may also play a role.

Figures 3(a) and 3(b) show DLTS spectra for different contacts on samples A1 and A2. For A1, the temperature positions and amplitudes of the peaks exhibit a considerable variation between the different contacts, e.g., a shift of ~40 K in position for E6 between contacts 1 and 2. Moreover, depth profiles of E5 and E6 (not shown) reveal a strong increase in amplitude toward the surface and a concentration below the detection limit ($\sim 10^{14}$ cm^{-3}) for depths exceeding ~0.7 μm. These results support the previous conclusion that the polishing introduces several different types of defects with overlapping levels and/or highly localized damaged regions non-uniformly distributed over the wafer surface. In contrast, for sample A2, the spectra are reproducible with only minor variations between the different contacts (Fig. 3(b)).

The pronounced decrease in intensity of E5 and E6 after etching suggests that they occur in close proximity to the surface, consistent with previous reports in the literature for polishing-induced defects.[6,8] According to Refs. 5 and 7, open volume defects, such as V_{Zn} and the oxygen vacancy V_O, and complexes thereof prevail after polishing. Thus, it is tempting to suggest that E5 and E6 in sample A1 may be related to clusters of open-volume defects like multi-vacancy complexes with a broad band of energy levels. In sample A2, on the other hand, having a considerably lower and laterally more uniform concentration of defects than A1, E5, and E6 arise predominantly from point-like defects. In fact, employing calculations based on density-functional-theory, Janotti *et al.*[20] have predicted that the (2+/0) transition level of V_O is located ~1 eV below E_c, i.e., close to the positions of E5 and E6 and at least one of these levels may possibly be related to V_O. Further, the large electron capture cross section of the E5 level (Table I) indicates that it originates from a donor-like defect but no distinct electric field dependence has been observed due to a limited range of possible variations in the bias voltage.

In summary, mechanical polishing of n-type ZnO is demonstrated to form electrically active defects and to cause compensation/passivation of shallow donors in the vicinity of the surface (<700 nm). High-temperature DLTS measurements, benefiting from high-quality Pd Schottky contacts, unveil two dominant and broad electron states with centered energy positions at 1.0 eV and 1.2 eV below E_c, tentatively associated with vacancy related defect centers. Post-polishing etching in diluted HF removes the compensation/passivation of the shallow donors and the concentration of deep electron states is reduced by one order of magnitude concurrent with a sharpening of the DLTS peaks approaching the shape of that of point-like defects.

This work was supported by the Norwegian Research Council through the NanoMat (CONE project) and FRIENERGI programs.

[1]C. Jagadish and S. J. Pearton, Zinc Oxide Bulk, Thin Films and Nanostructures (Elsevier, Oxford, 2006).
[2]J. E. Bradby, S. O. Kucheyev, J. S. Williams, C. Jagadish, M. V. Swain, P. Munroe, and M. R. Phillips, Appl. Phys. Lett. **80**, 4537 (2002).
[3]D. Lucca, D. Hamby, M. Klopfstein, G. Cantwell, C. Wetteland, J. Tesmer, and M. Nastasi, in Annals of CIRP 50 (2001), p. 397.
[4]D. Lucca, D. Hamby, M. J. Klopfstein, and G. Cantwell, Phys. Status Solidi B **229**, 845 (2002).
[5]D. Lucca, C. Wetteland, A. Misra, M. Klopfstein, M. Nastasi, C. Maggiore, and J. Tesmer, Nucl. Instrum. Methods Phys. Res. B **219–220**, 611 (2004).
[6]D. W. Hamby, D. A. Lucca, and M. J. Klopfstein, J. Appl. Phys. **97**, 043504 (2005).
[7]Z. Takkouk, N. Brihi, K. Guergouri, and Y. Marfaing, Physica B **366**, 185 (2005).
[8]F. A. Selim, M. H. Weber, D. Solodovnikov, and K. G. Lynn, Phys. Rev. Lett. **99**, 085502 (2007).
[9]J. Mass, M. Avella, J. Jiménez, A. Rodríguez, T. Rodríguez, M. Callahan, D. Bliss, and B. Wang, J. Cryst. Growth **310**, 1000 (2008).
[10]S. Pearton, D. Norton, K. Ip, Y. Heo, and T. Steiner, Prog. Mater. Sci. **50**, 293 (2005).
[11]R. Schifano, E. V. Monakhov, U. Grossner, and B. G. Svensson, Appl. Phys. Lett. **91**, 193507 (2007).
[12]Q. Gu, C. Ling, X. Chen, C. Cheng, A. Ng, C. Beling, S. Fung, A. B. Djurišić, and L. Lu, Appl. Phys. Lett. **90**, 122101 (2007).
[13]W. Mtangi, F. Auret, C. Nyamhere, P. J. van Rensburg, A. Chawanda, M. Diale, J. Nel, and W. Meyer, Physica B **404**, 4402 (2009).
[14]B. G. Svensson, T. M. Brseth, K. Johansen, T. Maqsood, R. Schifano, U. Grossner, J. Christensen, L. Vines, P. Klason, and Q. Zhao, Mater. Res. Soc. Symp. Proc. **L04**, 1035 (2008).
[15]L. Vines, E. Monakhov, R. Schifano, W. Mtangi, F. D. Auret, and B. Svensson, J. Appl. Phys. **107**, 103707 (2010).
[16]B. G. Svensson, K.-H. Rydén, and B. M. S. Lewerentz, J. Appl. Phys. **66**, 1699 (1989).
[17]U. Grossner, S. Gabrielsen, T. M. Brseth, J. G. amd A. Y. Kuznetsov, and B. G. Svensson, Appl. Phys. Lett. **85**, 2259 (2004).
[18]R. Schifano, E. V. Monakhov, B. G. Svensson, W. Mtangi, P. J. van Rensburg, and F. D. Auret, Physica B **404**, 4344 (2009).
[19]V. Quemener, L. Vines, E. Monakhov, and B. Svensson, Int. J. Appl. Ceram. Technol. (to be published).
[20]A. Janotti and C. G. V. de Walle, Phys. Rev. B **76**, 165202 (2007).

Paper III

Evolution of deep electronic states in ZnO during heat treatments in oxygen- and zinc-rich ambients.

V. Quemener, L. Vines, E.V. Monakhov and B.G. Svensson.

Accepted for publication in Appl. Phys. Lett.

Evolution of deep electronic states in ZnO during heat treatment in oxygen- and zinc-rich ambients

V. Quemener,[1, a)] L. Vines,[1] E.V. Monakhov,[1] and B.G. Svensson[1]
University of Oslo, Department of Physics/Center for Materials Science and Nanotechnology, P.O. Box 1048 Blindern, N-0316 Oslo, Norway

(Dated: 24 February 2012)

Hydrothermally grown ZnO samples have been annealed in Ar, Zn-rich and O-rich ambients and investigated by deep level transient spectroscopy (DLTS). The DLTS measurements reveal up to 6 different defect levels in the band gap after the different annealing conditions. A clear correlation has been found between the annealing treatment and the formation/suppression of two deep defect levels at ∼0.2 and ∼0.5 eV below the conduction band edge (E_c). As a result, the $E_c - 0.5\,eV$ level is assigned to a Zn-rich defect while the $E_c - 0.2\,eV$ level is due to a O-rich defect, where the latter shows donor behavior as revealed by a distinct Poole-Frenkel effect.

Zinc oxide (ZnO) exhibits attractive properties such as a direct wide band gap and a high excitonic binding energy that can be exploited in a number of applications of semiconductor and optoelectronic devices.[1] However, the use of ZnO is hampered by the presence of impurities and intrinsic defects causing a native n-type conductivity, which dramatically affects the electrical and optical performances. Thus, controlling these defects, during growth and device processing, is crucial. Electrically, several defect levels have been observed in the 20-600 meV range below the conduction band edge (E_c) and reported in the literature.[2–6] However, the origin of the defect levels remains unknown and extensive investigations need to be pursued to determine their identities. Several of the primary intrinsic defects are expected to be electrically active and play an important role in the n-type conductivity (see, for instance, Ref.[7]). Moreover, the formation energies depend on the chemical potential, resulting in different equilibrium concentrations of defects for O- and Zn-rich conditions. Post-growth annealing in various ambients may therefore alter the concentration of important (elementary) intrinsic defects, and can provide information on the origin of electronic states occurring in the band gap.

Previous studies by photoluminescence measurements (PL) have demonstrated a clear correlation between the position of the deep band emission and the Zn/O annealing conditions.[8–10] The formation of such deep bands is illustrated by a well known effect where ZnO turns reddish during Zn ambient annealing at 1100°C.[11–13] The red coloration has been attributed to Zn interstitials, (Zn_i) and/or oxygen vacancies (V_O),[12] and it can be removed by annealing in oxygen ambient. Most recently, Weber et al.[13] discussed the role of hydrogen in conjunction with oxygen deficient defects like hydrogen on O-site (H_O), and its possible association with the red coloration. The formation/suppression of defects related to O- or Zn-rich conditions has also been investigated by positron annihilation spectroscopy (PAS), and signatures for V_O-related and Zinc vacancy related complexes ($V_{Zn} - X$) have been identified.[12,14]. Studies of electrical signatures of defects related to O- or Zn-rich conditions have been scarce in the literature using spectroscopic techniques like deep level transient spectroscopy (DLTS), and so far, only one defect level at ∼0.5 eV below E_c has been reported to show a clear correlation with the annealing conditions.[3,9]

In the present work, the effect of annealing in Zn and in O-rich ambients on the defect evolution has been investigated by electrical techniques such as capacitance versus voltage (C-V) measurements and DLTS in the 30-400K temperature range. A clear correlation is revealed between the annealing treatments and the formation/suppression of two prominent deep levels in the upper part of the band gap; one is donor-like and associated with a O-rich (Zn-deficient) defect while the other arises from a Zn-rich (O-deficient) defect.

Two hydrothermally grown ZnO wafers from SPC Goodwill, labelled A and B, were heat treated in Argon (Ar) atmosphere at 1400°C during 1 hour to reduce the lithium (Li) content and obtain a net carrier (electron) concentration of $\sim 10^{17}\ cm^{-3}$, using a process described in detail elsewhere.[15,16] Before Schottky contact deposition, the samples were cleaned in acetone (5 min duration) and isopropanol (5 min) in an ultrasonic bath and then treated in a boiling 40% hydrogen peroxide (H_2O_2) solution for 1 min. Schottky barrier contacts were prepared on the Zn-polar face by depositing 100 nm thick Pd contacts using electron beam evaporation of a 99.999 % pure Pd source through a molybdenum shadow mask at a base pressure of 10^{-6} mbar. Silver paste was used as Ohmic contact on the back side (O-face). After a first set of current versus voltage (I-V), C-V and DLTS measurements, labelled A0 and B0, the contacts were removed by a gentle polishing using a rotating disc and diamond slurry with grain sizes of 0.25 μm, and etched in a 2% hydrofluoric acid solution (HF) for 2 min; this was performed in order to minimize the amount of interface defects formed by the polishing.[17] Then, the two samples were treated either in an oxygen or zinc ambient and electrically characterized employing Pd Schottky contacts prepared by the procedure previously described. Sam-

a)Electronic mail: vincent.quemener@smn.uio.no

TABLE I. Resistivity, obtained from four point probe measurements, and effective carrier concentration, obtained from C-V measurements, of sample A and B after different annealing conditions.

Sample	Annealing	resistivity ρ (Ωcm)	N_D (cm^{-3})
A0	Ar, 1400°C, 1h	0.66	5×10^{16}
A1	Zn, 1100°C, 30min	0.05	1×10^{17}
A2	O_2, 1100°C, 1h	0.60	8×10^{16}
B0	Ar, 1400°C, 1h	0.70	2×10^{17}
B1	O_2, 1100°C, 1h	0.65	1×10^{17}
B2	Zn, 1100°C, 30min	0.04	3×10^{17}

ple A was annealed at 1100°C during 30 min in a sealed quartz ampoule holding 99.99% Zn metal (measurement A1), while the sample B was annealed at 1100°C during 1 hour in flowing oxygen atmosphere (measurement B1). In order to distinguish between effects caused by the annealing ambient and those from other processing variations, the samples were, finally, annealed under the opposite conditions where sample A was treated in O-rich (measurement A2) and sample B in Zn-rich conditions (measurement B2). A survey of the different processes applied to samples A and B is given in Table I.

The I-V and C-V measurements were performed in darkness at room temperature using a Keithley 617 electrometer and a 1 MHz capacitance meter (HP 4280A), respectively. The I-V results showed stable rectifying behavior of about 3-4 orders of magnitudes for all the contacts on each sample. The DLTS measurements were performed in the temperature range 20K-400K with a reverse bias voltage of -3V and a pulse voltage of 3V (50 ms duration) using a refined version of the setup described in Ref.[18]. The DLTS signal was extracted applying a lock-in weighting function with different rate windows in the range $(20\text{ms})^{-1}$ to $(3200\text{ms})^{-1}$.

The carrier concentrations as well as the resistivities for the two samples after annealing in Ar, Zn-rich and O-rich conditions are summarized in Table I. After 1400°C in Ar atmosphere, the resistivity (ρ) is reduced by about 3 orders of magnitude, relative to the as-grown state. The carrier concentrations for A0 and B0 are $\sim 5 \times 10^{16}\, cm^{-3}$ and $2 \times 10^{17} cm^{-3}$, respectively. After the annealing in Zn atmosphere (sample A1 and B2), a red coloration occurs as expected,[11–13] and ρ is reduced by one order of magnitude relative to that for A0 and B0. In contrast, after annealing in O_2 the samples A2 and B1 are transparent and the resistivity is close to that of A0 and B0.

Figure 1 shows DLTS spectra of samples A (Fig. 1a) and B (Fig. 1b) and the different annealing conditions influence strongly the defect intensities. After the treatment in Ar atmosphere (samples A0 and B0), three main levels appear in the 30-300K range, labelled E2, E3 and E4, with energy positions of $\sim E_c - 0.19$, $\sim E_c - 0.30$ and $\sim E_c - 0.54$ eV, respectively. These levels are commonly observed in hydrothermally annealed samples treated at high temperature and have previously been reported in

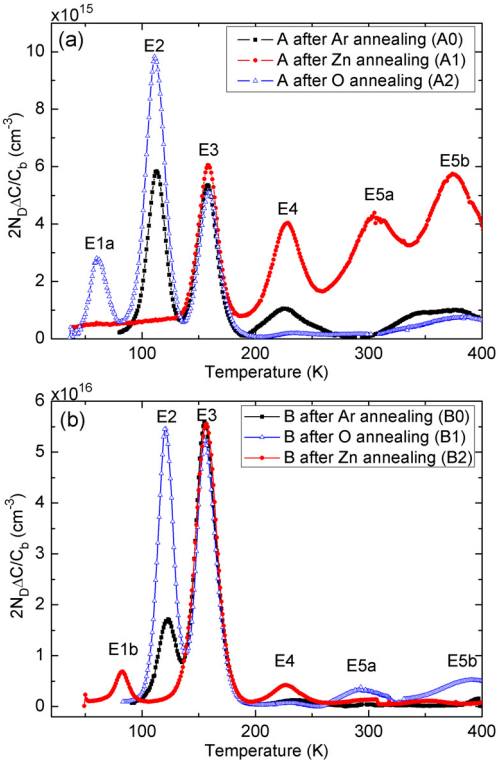

FIG. 1. (color online) DLTS spectra from samples A (a) and B(b) using rate windows of $(640\text{ms})^{-1}$ after different annealing processes. A reverse bias voltage of -3V and filling pulse voltage of 3V have been employed. C_b represents the reverse bias capacitance, N_D is the carrier concentration and ΔC is he amplitude of the capacitance transient.

the literature.[2,3,5,6] The energy positions and apparent capture cross sections are summarized in Table II.

After annealing in Zn- and O-rich conditions, new defect levels evolve, labelled E1a, E1b, E5a and E5b, with level positions of $\sim E_c - 0.10$, $\sim E_c - 0.11$, $\sim E_c - 0.72$ and $\sim E_c - 1.0$ eV, respectively (see Tab. II). However, the formation of E1a, E1b, E5a and E5b do not hinge on the annealing ambient; for sample A, E5a and E5b increase in amplitude after Zn annealing and then decrease after O annealing (samples A1 and A2), while for wafer B they increase after O annealing and then decrease after Zn annealing (samples B1 and B2). Hence, the evolution of E5a and E5b appear to be related to the annealing temperature and duration rather than to the ambient conditions. A similar conclusion holds also for E1a and E1b which grow more slowly with time than E5a and E5b and exhibit a higher stability.

The E3 defect shows a substantial difference in concentration between the nominally identical samples A0 and B0, implying that the detailed growth conditions have an important effect on its generation. This is also true for the net carrier (effective doping) concentration which is about a factor of 4 higher in sample B0 relative to A0 (see Tab. I). In fact, the concentration of E3 is $\sim 10\%$ of the effective dopant concentration in both A0 and B0. However, in contrast to that of the dopant concentration the strength of E3 does not vary with the different annealing treatments at 1100°C, indicating a high formation energy and high temperature stability. Indeed, the effect of heat treatment on E3 has previously been reported in the literature and shows that temperatures ≥ 1300°C are needed to influence the concentration of E3.[5,6]

The E2 and E4 defects depend strongly on the annealing conditions in a consistent manner for both samples A and B. Firstly, after annealing in Zn atmosphere (samples A1 and B2), E4 increases and E2 is removed below the detection limit. Secondly, after annealing in O_2 atmosphere (samples A2 and B1), E4 disappears and E2 increases strongly. It should be emphasized that the formation and annealing behaviors are systematic and reversible and do not depend on the sample history. Hence, it can be concluded that E2 is related to (or promoted by) an O-rich (Zn-deficient) defect like V_{Zn}, O_{Zn} and O_i, while the opposite holds for E4. The latter conclusion is consistent with the results in refs.[3] and[9], where an assignment of E4 to V_O was discussed. E4 displays almost identical concentrations in the samples A1 and B2, indicating that thermal equilibrium is indeed reached during the treatment in Zn-rich conditions and supporting an intrinsic origin of E4. The formation energy (E_{form}) of E4 can be estimated by $c/N_{sites} = exp(-E_{form}/kT)$, where c is the concentration of E4 and N_{sites} is the number of possible sites per unit volume, yielding a value of ~ 1.9 eV. This value is at least three times higher than that predicted for V_O by Vidya et al.[19], using a density-functional-theory-based pseudopotential all-electron method (without band gap correction), in n-type material (Fermi level position close to E_c) under Zn-rich conditions. However, a close agreement is obtained with the calculated value for Zn_i (~ 2.0 eV) and hence, it is tempting to associate E4 with a defect involving Zn_i; albeit not Zn_i itself which is expected to be highly mobile even at low temperatures (~ 600°C)[20] and not readily detected as an isolated (single) defect.

Fig. 2 shows the DLTS signal of E2 under different reverse bias conditions and the peak position shifts toward lower temperature with increasing electric field. Thus, the rate of electron emission is enhanced by the external field due to distortion (lowering) of the defect potential well. Fig. 3 reveals a close proportionality between the shift in the apparent energy position and the square root of the electric field, as predicted by the so-called Poole-Frenkel effect.[21] In n-type material, only donor-like states display field-enhanced emission and not (single) acceptor-like ones which become neutral after electron emission; hence, it can be concluded that E2 arises from a donor-like defect. For E4, no electric field dependence is observed within the experimental accuracy, possibly suggesting an acceptor-like defect. However, no ambiguous conclusion can be made for E4[22] and in addition, the detection of a field-enhanced emission from E4 is not straight forward due to a rather broad peak width.

TABLE II. Survey of the energy position and apparent capture cross section of the observed defect levels.

Defect	$E_c - E_t$ (eV)	σ_{na} (cm^2)
E1a	0.10	3×10^{-15}
E1b	0.11	2×10^{-17}
E2	0.19	6×10^{-17}
E3	0.30	2×10^{-15}
E4	0.54	1×10^{-13}
E5a	0.72	1×10^{-15}
E5b	1.00	2×10^{-12}

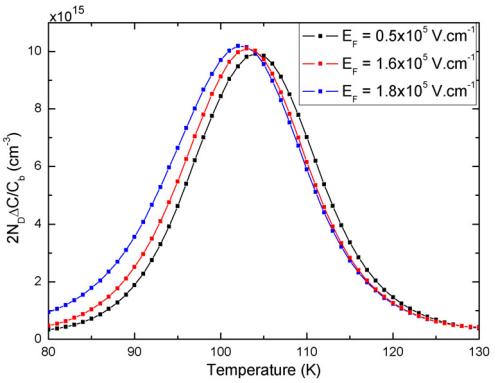

FIG. 2. (color online) DLTS spectra of E2 taken for different reverse bias of -1V, -3V and -4V corresponding to peak electrical fields of 0.5×10^5, 1.6×10^5 and 1.8×10^5 $V.cm^{-1}$, respectively.

The donor behavior of E2 does not immediately agree with the three prime intrinsic (O-rich) candidates: V_{Zn}, O_{Zn} and O_i.[20] However, O_i in the dumbbell configuration ($O_{i,db}$) is theoretically predicted to be donor-like, although with a level position close to the valence band edge.[23] The concentration of E2 varies by a factor $\sim$5 between the sample A2 and B1 (see Fig. 1), while the carrier concentration is the same within 25% (see Tab. I). This variation excludes a pure intrinsic nature of E2 and favours an impurity-related defect promoted by O annealing and suppressed by Zn annealing. According to results from secondary ion mass spectrometry (SIMS) measurements,[5] possible impurities are Al, Si, Mg, Fe, Mn and Ni but no further distinction can be made through correlation between the DLTS and SIMS data. Here, it should be emphasized that hydrogen,

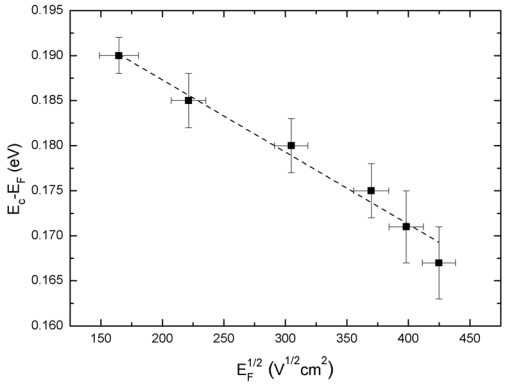

FIG. 3. Energy position of E2 defect level versus the square root of the electric field.

which is a prominent impurity in ZnO,[15] can be ruled out since similar samples as used in this study have been annealed in H-rich conditions with no effect on E2.[6]

Hydrothermally grown ZnO samples have been successively annealed in Ar, Zn and O-rich conditions. Strong correlations have been found between the annealing treatment and the formation/suppression of deep defect levels in the upper part of the band gap. It is found that a level at $E_c - 0.2$ eV, commonly labeled E2, can be ascribed to an impurity-related defect promoted by O-rich conditions, while a level at $E_c - 0.5$ eV, commonly labeled E4, is promoted by Zn-rich conditions and most likely due to a center governed by intrinsic (Zn_i) species. It is also demonstrated that the E2 level exhibits a clear Poole-Frenkel effect showing a donor nature.

This work was supported by the Norwegian Research Council through the NanoMat (CONE project) and FRIENERGI programs.

[1] C. Jagadish and S. J. Pearton. *Zinc Oxide Bulk, Thin Films and Nanostructures*. Elsevier, Oxford, 2006.
[2] F. D. Auret, S. A. Goodman, M. J. Legodi, W. E. Meyer, and D. C. Look. *Appl. Phys. Lett.*, 80:1340, 2002.
[3] T. Frank, G. Pensl, R. Tena-Zaera, J. Zúniga-Pérez, C. Martínez-Tomás, V. Munoz-Sanjosé, T. Ohshima, H. Itoh, D. Hofmann, D. Pfisterer, J. Sann, and B. Meyer. *Appl. Phys. A*, A 88:141–145, 2007.
[4] R. Schifano, E. V. Monakhov, B. G. Svensson, W. Mtangi, P. Janse van Rensburg, and F. D. Auret. *Physica B*, 404:4344–4348, 2009.
[5] L. Vines, E.V. Monakhov, and B.G. Svensson. *Physica B*, 404:4386, 2009.
[6] V. Quemener, L. Vines, E.V. Monakhov, and B.G. Svensson. *Int. J. Appl. Ceram. Technol.*, 8:1017, 2011.
[7] A. Janotti and C. G. Van de Walle. *Rep. Prog. Phys.*, 72:126501, 2009.
[8] T. Moe Børseth, P. Klason, Q. X. Zhao, M. Willander, B. G. Svensson, and A. Yu. Kuznetsov. *Appl. Phys. Lett.*, 89:262112, 2006.
[9] D. M. Hofmann, D. Pfisterer, J. Sann, B. K. Meyer, R. Tena-Zaera, V. Munoz-Sanjosé, T. Frank, and G. Pensl. *Appl. Phys. A*, 88:147, 2007.
[10] P. Klason, T. Moe Børseth, Q. X. Zhao, B. G. Svensson, A. Yu. Kuznetsov, P. J. Bergman, and M. Willander. *Solid State Commun.*, 145:321, 2008.
[11] W. Ehret and A. Greenstone. *J. Am. Chem. Soc.*, 65:872, 1943.
[12] F. A. Selim, M. H. Weber, D. Solodovnikov, and K. G. Lynn. *Phys. Rev. Lett.*, 99:085502, 2007.
[13] M. H. Weber and K. G. Lynn. *J. Phys. Conf. Ser.*, 262:012063, 2011.
[14] A. Zubiaga, F. Plazaola, J. A. García, F. Tuomisto, V. Munoz-Sanjosé, and R. Tena-Zaera. *Phys. Rev. B*, 76:085202, 2007.
[15] E.V. Monakhov, A. Yu Kuznetsov, and B.G. Svensson. *J. Appl. Phys. D*, 42:153001, 2009.
[16] L. Vines, E.V. Monakhov, R. Schifano, W. Mtangi, F. D. Auret, and B.G. Svensson. *J. Appl. Phys.*, 107:103707, 2010.
[17] V. Quemener, L. Vines, E. V. Monakhov, and B. G. *Appl. Phys. Lett.*, 99:112112, 2011.
[18] B. G. Svensson, K.-H. Rydén, and B. M. S. Lewerentz. *J. Appl. Phys.*, 66:1699, 1989.
[19] R. Vidya, P. Ravindran, H. Fjellvåg, B.G. Svensson, E. Monakhov, M. Ganchenkova, and R.M. Nieminen. *Phys. Rev. B*, 83:045206, 2011.
[20] A. Janotti and C. G. Van de Walle. *Phys. Rev. B*, 76:165202, 2007.
[21] J. Frenkel. *Phys. Rev.*, 54:647, 1938.
[22] W.R. Buchwald and N.M. Johnson. *J. Appl. Phys.*, 64:958, 1988.
[23] P. Erhart, K. Albe, and A. Klein. *Phys. Rev. B*, 73:205203, 2006.

Paper IV

Acceptor-like deep level defects in ion-implanted ZnO.

L. Vines, J. Wong-Leung, C. Jagadish, V. Quemener, E.V. Monakhov and B.G. Svensson.

Submitted in Appl. Phys. Lett.

Acceptor-like deep level defects in ion-implanted ZnO

L. Vines[1],* J. Wong-Leung[2], C. Jagadish[2], V. Quemener[1], E.V. Monakhov[1], and B.G. Svensson[1]

[1] *University of Oslo, Department of Physics/Centre for Materials Science and Nanotechnology, P.O. Box 1048 Blindern, N-0316 Oslo, Norway and*

[2] *Department of Electronic Materials Engineering, Research School of Physics and Engineering, The Australian National University, Canberra, ACT 0200, Australia*

(Dated: March 8, 2012)

Abstract

N-type ZnO samples have been implanted with 3 MeV and 6 MeV Zn^+ ions at room temperature to doses between 1×10^8 and 2×10^{10} cm^{-2}, and the defect evolution has been studied by capacitance-voltage (CV) and deep level transient spectroscopy (DLTS). Carrier concentration profiles from the CV measurements show a dose dependent compensation by acceptor-like defects along the implantation depth profile. At least four implantation-related deep-level defects arise, as observed by DLTS, with energy positions of 0.57, 0.89 ,1.06 and 1.2 eV below the conduction band edge. While the amplitude of the 0.57 eV level remains small, the strength of the 1.06 and 1.2 eV levels increase linearily with ion dose and they are attributed to intrinsic defects. The 0.89 eV level occurs as a shoulder on the low temperature side of the 1.06 eV peak, but the amplitude is reduced already after the first DLTS scan reaching 410 K. Moreover, a re-distribution of defects as a function of depth is observed after annealing below 400 K showing that prominent defect reactions, possibly involving migration, take place at modest temperatures.

* Lasse.Vines@fys.uio.no

Zinc oxide (ZnO) is a wide band gap semiconductor ($E_g \sim 3.4$ eV) that has received considerable attention during the past few years due to its potential applications in light emitting devices and photovoltaics. However, the technological advances of ZnO have been hindered by the difficulty in controlling and understanding the electrical behavior of intrinsic and impurity related defects. In particular, controlling charge carrier concentration profiles by ion implantation remains a major challenge for ZnO based devices. This includes both dopant activation in the desired atomic configuration and control of ion induced damage.

Studying irradiated or implanted samples is indispensable for the understanding of electrically active defects, both intrinsic and impurity related ones, where deep level transient spectroscopy (DLTS) is one of the most sensitive techniques. Intrinsic defects are of particular importance in ZnO, since many of those are expected to be electrically active and play an important role for the "native" n-type conduction and the difficulty in achieving p-type doping. However, only a few irradiation studies of ZnO using DLTS have been reported so far [1] [2] [3] [4]; in fact, most of the irradiation studies have been carried out using light projectiles such as electrons, protons and helium ions, mainly focusing on defects detectable below 300K. However, recent advances in the quality of Schottky contacts have made it possible to extend the DLTS temperature range up to 600 K and to probe deep into the band gap [5] [6].

Here, we report on 3 and 6 MeV Zn^+ implantation into ZnO in the low dose regime and several defect levels are observed above 300 K. Moreover, a re-distribution of defects occurs below 400 K, indicating a high mobility, consistent with an efficient dynamic annealing but possibly also with formation of large and more stable defect clusters.

Two wafers of hydrothermally grown ZnO (HT-ZnO) from Tokyo Denpa, labelled W1 and W2, were cut into four 5×5 mm samples. The samples were cleaned in acetone and ethanol, and treated for one minute in boiling H_2O_2 before 100nm thick Pd Schottky contacts were deposited using e-beam evaporation. The Schottky contacts showed a rectification of the current by 2-4 orders of magnitude between forward and reverse bias. The samples were then implanted at room temperature using 3MeV Zn^{3+} ions for the W1 samples and 6 MeV Zn^{6+} ions for the W2 samples, and with doses ranging from 1×10^8 to $2 \times 10^{10}\, cm^{-2}$. One sample of each wafer was left as reference (non-implanted) and no influence of the implantation dose on the rectifying behavior of the Schottky contacts was found. The projected range (R_p) of the Zn ions was $\sim 1.0\mu m$ and $\sim 1.9\mu m$ for the 3 and 6 MeV

implantations, respectively, as estimated by simulations using the SRIM code[7]. As an example, the peak Zn concentration for the 6 MeV implantation and a dose of 5×10^8 cm^{-2} is $\sim 1.5 \times 10^{13}\, cm^{-3}$. After implantation, the samples were stored in a freezer (-20°C) until measured. DLTS was carried out while scanning up in temperature using a refined version of a setup described in Ref. [8]. A reverse bias of $-3\,V$ was used with a filling pulse of $+3\,V$ and 5 ms duration.

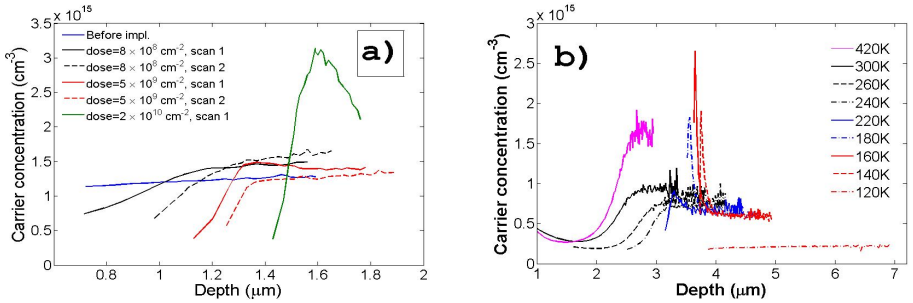

FIG. 1. Carrier concentration versus depth profiles for a) W1-samples implanted by 3 MeV Zn ions to different doses, and b) W2-sample implanted with 6 MeV Zn ions to a dose of 1.2×10^9 cm^{-2} and analysed at different temperatures after scan 2 (probing frequency = 1MHz).

Figure 1(a) shows the charge carrier concentration (N_d) versus depth extracted from capacitance-voltage (CV) measurements at 300 K for the W1 samples implanted with doses between 8×10^8 and $2 \times 10^{10}\, cm^{-2}$; scan 1 is the first one after implantation. Before implantation, $N_d \sim 1.2 \times 10^{15}\, cm^{-3}$ and is uniform as a function of depth. The sample implanted with the low dose ($8 \times 10^8\, cm^{-2}$) shows only minor changes in the charge carrier distribution (scan 1), but a significant redistribution takes place for the medium (4×10^9 cm^{-2}) and high ($2 \times 10^{10}\, cm^{-2}$) dose samples. For the highest dose, a strongly reduced charge carrier concentration occurs around R_p followed by a pronounced increase below R$_p$. This increase is not real and attributed to an anomaly occuring when profiling nonuniform distributions of deep acceptor-like centers [9]. Indeed, Fig. 1(b) shows the carrier concentration, after DLTS scan 2, at different temperatures using a probing frequency of 1MHz and sweep frequency of 5 Hz; in accordance with Kimerling [9], the anomalous overshoot below R_p occurs only at certain temperatures, i.e., when the emission rate from the deep acceptor is intermediate to the sweep rate and the probing rate.

Further, Fig. 1(a) reveals a considerable re-distribution or generation of defects between the as-implanted (scan 1) and $\sim$ 410K annealed profiles (scan 2), where N_d in the near-surface region decreases after annealing and with increasing dose. For the high dose sample (2×10^{10} cm^{-2}), a complete freeze-out of N_d occurs in scan 2. Scan 3 remained similar to scan 2, and for clarity, data are not included in the figure. Moreover, the as-grown samples did not show a reduced carrier concentration in the near surface region or a change in the profile after successive DLTS scans (not shown). Thus, an acceptor activation or donor removal occur in the implanted samples during the first scan, demonstrating that migration or defect reactions take place below 420 K. For instance, theory predicts that zinc interstitials (Zn_I) have a migration barrier of $\sim$ 0.6 eV [10], indicating that they are mobile around room temperature, and can readily migrate towards the bulk or the surface during the first scan.

Another species with high mobility, and abundant in ZnO, is hydrogen (H) [11][12], which may act as a donor and/or passivant of acceptors. Interstitial H is usually regarded to have a migration energy of $\sim$ 0.8 eV [13][14][15], i.e., sufficiently low to enable migration lengths in excess of 100 nm during scan 1. The CV-profiles show an evolution of deep acceptor centers after scan 1 implying that donor-like defects like Zn_I and H_O/H_I do not play a direct role. However, activation of H-passivated acceptors with states in the upper part of E_g can not be excluded, although H is not expected to leave the damaged region around R_p, but rather form more stable complexes [16]. Further, the reduction in N_d at R_p is at least a factor of 5 higher than the concentration of implanted Zn showing that ion-induced defects are involved in the evolution/activation of deep acceptors, possibly in combination with an abundant impurity, like H.

Figure 2 shows DLTS spectra for the W1 and W2 samples taken immediately after implantation (scan 1). At least four levels are present, labeled E3-E6. The spectrum for the highest dose sample ($2 \times 10^{10}\ cm^{-2}$) is omitted due to the strong carrier compensation, as evident from Fig. 1, but it follows the same trend as the other samples. A pronounced peak of the well-known level around $E_c - 0.3\ eV$ (E_c denotes the conduction band edge), normally labeled E3[17], is found in the as-grown samples, and the strength varies by more than a factor of two between the two wafers. However, the amplitude of E3 does not change significantly after implantation. The level labeled E4, with a position of $E_c - 0.57$ eV, has also been reported previously[17], and tentatively assigned to the oxygen vacancy (V_O) [18]. Interestingly, the concentration of E4 is low in the present samples, in contrast to that re-

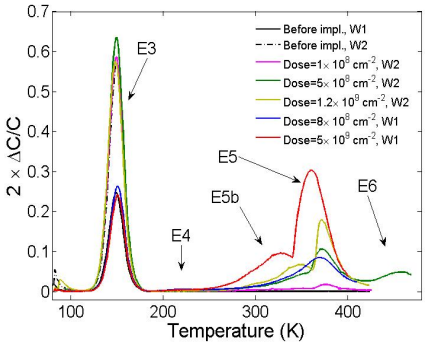

FIG. 2. DLTS signal ($2 \times \Delta C/C$) for samples before and after implantion with 3 MeV (W1) and 6 MeV (W2) Zn to doses from 1×10^8 to 5×10^9 cm^{-2}.

ported by other authors after electron and light ion irradiation [1, 3]. This casts doubts on the identification of E4 as V_O, since V_O is a primary defect, and anticipated to increase in concentration with ion dose.

Less is known about the level labeled E5, with an energy position of ~ 1.06 eV below E_c, since DLTS results above room temperature are scarce in the literature, primarely because of poor quality Schottky contacts[5]. In most of the as-implanted samples, the E5 peak is accompanied by a shoulder on the low temperature tail, labeled E5b, and with a position of $\sim E_c - 0.90eV$. Both E5 and E5b exhibit a strong dose dependence, where the concentration of E5 in samples implanted with 1.2×10^9 ions/cm^2, or higher, exceeds the maximum limit ($\lesssim 10\%$ of N_d) for a quantitative DLTS analysis. As a result, charge carrier freeze out by E5 becomes substantial and the peak position shifts towards lower temperatures in the highest dose sample (5×10^9 cm^{-2}) [19]. The assymetric shape of the E5 peak, with a sharp rise on the low temperature side, should be noticed but further investigations are needed to clarify the origin of this behavior.

An even deeper level, E6, exists in the 5×10^8 cm^{-2} sample where the upper temperature of the DLTS scan was extended to 460K. The extracted energy position is $\sim E_c - 1.2\,eV$, based on data for 3 rate windows covering the E6 peak within 460 K. Interestingly, two levels similar to E5 and E6, appearing in the same temperature range and with similar energy positions, have been observed in samples exposed to mechanical polishing [5]. This suggests an intrinsic origin of E5 and E6 and their general importance in processing of ZnO.

In Ref. [5], they were tentatively assigned to vacancies or clusters thereof.

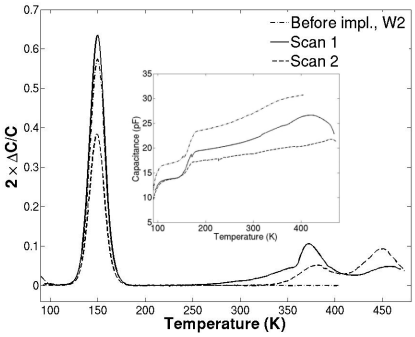

FIG. 3. DLTS signal ($2 \times \Delta C/C$) versus temperature for a W2 sample before and after implantion with 6MeV Zn ions to a dose of 5×10^8 cm^{-2}, scans 1 and 2 are successive ones (up to 460 K) after the implantation.

Figure 3 shows DLTS spectra of the W2 sample before and after implantation with 6 MeV Zn ions to a dose of 5×10^8 cm^{-2}. The inset in Fig. 3 displays the corresponding steady-state capacitance versus temperature. Several DLTS scans subsequent to scan 2 were also carried out, but they yielded similar results as those of scan 2. Fig. 3 reveals a change in both concentration and peak position of E5, E5b and E6 between the different scans. E5b appears to be highly unstable above $\sim$ 400K and disappears. E5 is reduced by $\sim 50\%$ and shifts towards higher temperatures, while E6 exhibits an increase of similar magnitude as the loss of E5. The reduction in reverse bias capacitance revealed by the inset of Fig. 3 complies with the results in Fig. 1, indicating activation/evolution of deep acceptors after the implant. Moreover, the temperature dependence of the electron emission rates from E5 and E5b deduced from scan 1 do not follow a strict Arrhenius behavior, suggesting that multiple levels may be present. However, for the subsequent DLTS scan (scan 2), an Arrhenius behavior is obeyed, and the estimated energy level positions stated above are taken from scan 2.

The strong generation of E5 (and E6) as a function of ion dose unveiled by Fig. 2 is striking, and the increase in amplitude exhibits a close to linear dose dependence. However, for a fully quantitative analysis profiling measurements are required. Figure 4 illustrates such profiles of E3, E5 and E6 for the samples implanted with 5×10^8 and 1.2×10^9 ions/cm^2,

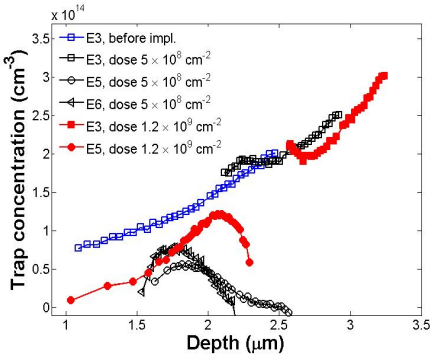

FIG. 4. Concentration versus depth profiles of E3, E5 and E6 for the W2 samples implanted with 6 MeV Zn ions to doses of 5×10^8 and 1.2×10^9 cm^{-2}, where the λ-effect have been taken into account.

while the amplitude of E4 is too low for reliable measurements. E3 displays an increasing concentration towards the bulk, and no dependence on ion dose is revealed. These results are fully consistent with the DLTS amplitudes of E3 in Figs. 2 and 3 and also with previous studies in the literature [2] [3] [17], indicating that irradiation has a weak (if any) effect on the strength of E3. The strong E3 signal prior to implantation limits the accuracy of the extracted generation rate, but it is at least one order of magnitude lower than that of E5 and close to zero (within the experimental accuracy).

In contrast to E3, both E5 and E6 show a clear peak in the concentration around R_p (Fig. 4) and they are evidently implantation induced. From SRIM simulations [7], and assuming a displacement threshold energy of 30 and 52 eV for Zn and O atoms, respectively [20], the total peak vacancy generation is found to be 1.2 vacancies/ion/Å. For E6, the generation rate is found to be 9×10^{-4} centers per vacancy, which is more than one order of magnitude lower than the corresponding rate of the vacancy-oxygen pair and the divacancy center in Si [21]. Hence, one may argue that E6 arises from a complex rather than a primary (low-order) defect; on the other hand, ZnO is well known to exhibit pronounced dynamic annealing [22], and a primary defect cannot be excluded. The concentration of E6 reaches a maximum close to R_p, with a rapid reduction towards the surface. Interestingly, the decrease towards the surface is sharper than that of the vacancy profile, as estimated by SRIM, and resembles more the implantation profile. In implanted layers, it is well established that the

region deeper than R_p is interstitial rich, while the more shallow region is vacancy rich, see for example Ref. [23]. Thus, it may be speculated that E6 is related to interstitials (Zn_I and/or O_I) rather than to vacancies (V_{Zn}, V_O).

In contrast, E5 has a clear surface tail, possibly suggesting a vacancy related center, in agreement with Ref. [5] and positron annihilation studies [24]. The peak generation rate of E5 is similar to that of E6, i.e. $\sim 9 \times 10^{-4}$ centers/vacancy and this value holds irrespective of ion dose confirming a linear dose dependence (Fig. 2). The linear dependence implies a dilute regime where the concentration of stable defects is not high enough to influence the trapping of migrating defects from neighbouring ion tracks [21]. Hence, E5 originates most likely from a primary defect of vacancy-type or a low-order vacancy cluster formed directly in single collision cascades.

In summary, n-type ZnO samples have been implanted with 3 and 6 MeV Zn^+ ions using doses between 8×10^8 and 2×10^{10} cm^{-2}, and the generation of electrically active defects has been studied by DLTS. C-V measurements show charge carrier compensation by deep acceptor-like traps evolving at depths $\lesssim R_p$ during modest post-implant annealing ($\sim$ 400 K). At least four implantation-induced deep-level defects arise, with energy positions of 0.57, 0.89, 1.06 and 1.2 eV below E_c. The two latter ones are scarcely reported for implanted/irradiated samples and both exhibit a generation rate of $\lesssim 1 \times 10^{-3}$ centers per vacancy (or interstitial) in the region around R_p. Based on their concentration-versus-depth profiles, it is argued that E5 is possibly vacancy-related while E6 is tentatively associated with interstitials.

This work was supported by the Norwegian Research Council through the Frienergi program and the Australian Research Council through the Discovery projects program.

[1] F. D. Auret, S. A. Goodman, M. Hayes, M. J. Legodi, H. A. van Laarhoven, and D. C. Look, Appl. Phys. Lett. **79**, 3074 (2001).

[2] M. Hayes, F. D. Auret, P. J. Janse van Rensburg, J. M. Nel, W. Wesch, and E. Wendler, phys. stat. sol. (b) **244**, 1544 (2007).

[3] M. Hayes, F. D. Auret, P. J. Janse van Rensburg, J. M. Nel, W. Wesch, and E. Wendler, Nucl. Instr. Met. Phys. Res. B **257**, 311 (2007).

[4] Z.-Q. Fang, B. Claflin, D. C. Look, and G. C. Farlow, J. Appl. Phys. **101**, 086106 (2007).

[5] V. Quemener, L. Vines, E.V. Monakhov, and B.G. Svensson, Appl. Phys. Lett. **99**, 112112 (2011).

[6] L. J Brillson and Y. Lu, J. Appl. Phys. **605**, 121301 (2011).

[7] J.F. Ziegler, J.P. Biersack, and U. Littmark, *The stopping and Range of Ions in Solids* (Pergamon, New York, 1985).

[8] B.G. Svensson, K.-H. Rydén, and B.M.S. Lewerentz, J. Appl. Phys. **66**, 1699 (1989).

[9] L. C. Kimerling, J. Appl. Phys. **45**, 1839 (1974).

[10] A. Janotti and C.G. Van de Walle, Phys. Rev. B **75**, 165202 (2007).

[11] E. Mollwo, Z. Phys. **138**, 478 (1954).

[12] S.F.J Cox, E. A. Davis, S. P. Cottrell, P.J.C. King, J. S. Lord, J. M. Gil, H. V. Alberto, R. C. Vilao, J. Piroto Duarte, N. Ayres de Campos, A. Weidinger, R. L. Lichti, and S. J.C. Irvine, Phys. Rev. Lett **86**, 2601 (2001).

[13] D. G. Thomas and J. J. Lander, J. Chem. Phys. **25**, 1136 (1956).

[14] N. H. Nickel and K. Brendel, Phys. Rev. B **68**, 193303 (2003).

[15] K. M.Johansen, J. S. Christensen, E. V. Monakhov, A. Yu. Kuznetsov, and B. G. Svensson, Appl. Phys. Lett. **93**, 152109 (2008).

[16] E. V. Monakhov, J. S. Christensen, K. Maknys, B. G. Svensson, and A. Y. Kuznetsov, Appl. Phys. Lett. **87**, 191910 (2005).

[17] F. D. Auret, S. A. Goodman, M. J. Legodi, W. E. Meyer, and D. C. Look, Appl. Phys. Lett. **80**, 1340 (2002).

[18] T. Frank, G. Pensl, R. Tena-Zaera, J. Zúñiga-Pérez, C. Matńez-Tomás, V. Muñoz-Sanjosé, T. Ohshima, H. Itoh, D. Hofmann, D. Pfisterer, J. Sann, and B. Meyer, Appl. Phys A **88**, 141 (2007).

[19] E.V. Monakhov, J. Wong-Leung, A.Yu. Kuznetsov, C. Jagadish, and B.G. Svensson, Phys. Rev. B **65**, 245201 (2002).

[20] R. E. Williford, R. Devanathan, and W.J. Weber, Nucl. Instr. Met. Phys. Res. B **141**, 94 (1998).

[21] B. G. Svensson, C. Jagadish, A. Hallén, and J. Lalita, Phys. Rev. B **55**, 10498 (1997).

[22] C. Jagadish and S. J. Pearton, eds., *Zinc Oxide Bulk, Thin films and Nanostructures* (Elsevier, Oxford, 2006).

[23] P. Lèvègue, H. Kortegaard Nielsen, P. Pellegrino, A. Hallèn, B.G. Svensson, A. Yu. Kuznetsov, J. Wong-Leung, C. Jagadish, and V. Privitera, J. Appl. Phys. **93**, 871 (2003).

[24] F. A. Selim, M. H. Weber, D. Solodovnikov, and K.G. Lynn, Phys. Rev. Lett. **99**, 085502 (2007).

Paper V

Electronic properties of n-ZnO(Al)/p-Si heterojunction prepared by dc magnetron sputtering.

V. Quemener, L. Vines, E.V. Monakhov and B.G. Svensson.

Thin Solid Films, 519 (2011) 5763-5766

Paper VI

Electronic properties of ZnO/Si heterojunction prepared by ALD.

V. Quemener, M. Alnes, L. Vines, O. Nilsen, H. Fjellvåg, E.V. Monakhov and B.G. Svensson.

Solid State Phenomena. 178-179 (2011) 130-135

Paper VII

The work function of n-ZnO deduced from heterojunctions with Si prepared by ALD.

V. Quemener, M. Alnes, L. Vines, P. Rauwel, O. Nilsen, H. Fjellvåg, E.V. Monakhov and B.G. Svensson.

To be submitted in J. Appl. Phys.

The work function of n-ZnO deduced from heterojunctions with Si prepared by ALD

V. Quemener,[1, a)] M. Alnes,[2] L. Vines,[1] P. Rauwel,[3] O. Nilsen,[2] H. Fjellvåg,[2] E.V. Monakhov,[1] and B.G. Svensson[1]

[1)] *Department of Physics/Centre for Materials Science and Nanotechnology, University of Oslo, P.O. Box 1048 Blindern, N-0316 Oslo, Norway*

[2)] *Department of Chemistry/Centre for Materials Science and Nanotechnology, University of Oslo, P.O. Box 1048 Blindern, N-0316 Oslo, Norway*

[3)] *Center for Materials Science and Nanotechnology, University of Oslo, P.O. Box 1126 Blindern, N-0318 Oslo, Norway*

(Dated: 9 March 2012)

Highly doped n-type ZnO films have been grown on n-type and p-type Si substrates by atomic layer deposition. Transmission electron microscopy shows columnar growth of the ZnO films with randomly oriented grains and a very thin interfacial layer of SiO_x ($x \leq 2$) with a thickness below 0.4 nm to the Si substrate. Current-voltage and capacitance-voltage measurements performed at temperatures from 50 to 300K reveal a strong rectifying behavior on both types of substrates with an ideality factor close to unity between 180 and 280K. Using the classical approach of thermionic emission, the barrier heights of the ZnO/n-Si and ZnO/p-Si junctions have been deduced and consistent values are obtained yielding a work function of n-type ZnO close to 4.65 eV.

Keywords: Zinc oxide, Silicon, Interface, Work function

[a)] Electronic mail: vincent.quemener@smn.uio.no

I. INTRODUCTION

Zinc oxide (ZnO) is a direct wide band gap semiconductor (Eg = 3.37 eV at room temperature) with several appealing properties, and it can be used, for instance, as a transparent conducting layer in optoelectronic devices.[1] Further, ZnO can form rectifying junctions with other semiconductors like silicon and such heterostructures may have considerable interest for photovoltaic systems. However, the performance and efficiency of ZnO/Si heterojunctions are limited by the presence of defects and/or a SiO_x ($x \leq 2$) layer at the interface. Thus, controlling the interface oxide layer and minimizing charge carrier recombination are crucial issues to enhance the performance of ZnO/Si heterostructures. Here, the use of 'soft' thin film deposition techniques, like Atomic Layer Deposition (ALD)[2–4] with a minimum of defect formation, is a necessity.

In order to design ZnO/Si heterostructures with optimum properties and predict their electrical and optical characteristics, the work function of ZnO (Φ_{ZnO}), which also is of fundamental interest, needs to be known with a high degree of accuracy. Values reported in the literature for Φ_{ZnO} show a large scatter; results from Kelvin probe[5–8] and XPS[9–12] measurements are in the 3.5-5.2 eV range and depend on the process conditions used. Values extracted from barrier heights ($\Phi_{bn,p}$) deduced by electrical transport studies of heterojunctions, employing current versus voltage (I-V) and capacitance versus voltage (C-V) measurements, are in the 4.3-4.9 eV range.[13–19] In the majority of these studies, the ZnO films have been deposited by rather 'violent' techniques, like reactive RF sputtering[13–16], suffering from the inherent limitation of defect generation at the interface.[20,21] Results from investigations of $\Phi_{bn,p}$ and Φ_{ZnO} using 'soft' deposition techniques, like ALD, are scarce in the literature.

In the present work, the layer structure, electronic properties and electrical transport mechanisms of ZnO/n-Si and ZnO/p-Si heterojunctions prepared by ALD have been investigated. The structure of the ZnO films and the interfacial layer with Si were studied by cross sectional transmission electron microscopy (TEM) and the electrical properties were determined by Hall effect, I-V and C-V measurements undertaken at different temperatures (TDH, I-V-T and C-V-T). An interface layer of SiO_x ($x \leq 2$) with a thickness of only ≤ 0.4 nm is demonstrated, which is substantially lower than that previously reported in the literature.[15,22–24] Applying the classical thermionic-emission theory for the current transport

across the ZnO/Si junction, self-consistent values of $\Phi_{bn,p}$ and Φ_{ZnO} have been obtained from the experimental data.

II. EXPERIMENTAL

ZnO films were deposited by ALD, using a F-120 Sat reactor (ASM Microchemistry), on cleaned and HF etched (100) n-type and p-type Si wafers with resistivities of about 240 Ωcm and 50 Ωcm, respectively. The precursors used were diethyl zinc $Zn(CH_2CH_3)_2$ (DEZ) (EMF Speciality Chemicals) and deionized water (H_2O). The precursors were introduced into the reactor at a base pressure of 3.5 mbar, at room temperature and with a substrate temperature of 175°C. One ALD cycle consisted of 0.2 s pulse of DEZ, 2.5 s purge with N_2, 1.0 s pulse of H_2O and 4.0 s purge with N_2. The ALD cycle was repeated 1375 times, and the growth rate was ∼0.15 nm/cycle. For the I-V and C-V characterizations, 100 nm thick Nickel (Ni) contacts were deposited on the ZnO films using electron beam evaporation from a 99.999% pure Ni source through a molybdenum shadow mask at a base pressure of 10^{-6} mbar. The circular Ni contacts had a diameter of 1 mm and served as Ohmic contacts and lithographic mask for the ZnO films. After deposition, the samples were dipped in a 2% HF solution for 30 s in order to pattern the ZnO layer. The I-V and C-V measurements were performed in dark in the 50-300K temperature range using a Keithley 6487 electrometer and a 1 MHz Boonton 7200 capacitance meter, respectively. From C-V measurements, carrier concentrations of $N_D = 2 \times 10^{13}\, cm^{-3}$ and $N_A = 8 \times 10^{14}\, cm^{-3}$ for the n-type and p-type Si substrates, respectively, were deduced in accordance with their nominal resistivity values.

The TDH measurements were conducted using a Lakeshore 7704A setup operating in the 20-300K temperature range and applying indium as Ohmic contact to ZnO films deposited on glass and Si substrates. The crystal and layer structure of the samples was investigated by cross sectional TEM on a JEOL 2010FS instrument operating at 200 KV and disposing a point to point resolution of 1.9 Å. Thin foils were prepared by mechanical thinning by the Tripod method, followed by ion milling to obtain electron transparency.

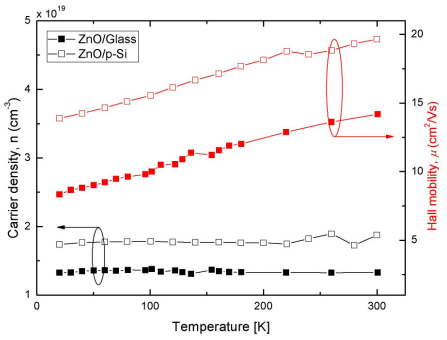

FIG. 1. (color online) Results from TDH measurements of ZnO films deposited on glass (filled symbols) and on p-type Si substrates (open symbols).

III. RESULTS AND DISCUSSION

Figure 1 compares results from TDH measurements of ZnO films deposited on glass and p-type Si substrates. In the latter case, a constant carrier concentration of $\sim 10^{19}\, cm^{-3}$ is obtained with an increasing mobility as a function of temperature reaching $\sim 20\, cm^2 V^{-1} s^{-1}$ at 300K. The impurity content of the ZnO films has been investigated by secondary ion mass spectrometry, where the main impurities observed are hydrogen ($\sim 5 \times 10^{20}\, cm^{-3}$) and carbon ($\sim 2 \times 10^{19}\, cm^{-3}$) (not shown) coming from the precursors used during the ALD growth. Other impurities, such as Si and Al, are also present but with concentrations below $10^{17}\, cm^{-3}$. Thus, the n-type doping is mainly assigned to hydrogen and/or hydrogen related complexes.[25,26] The constant carrier concentration as a function of temperature (Fig. 1) implies strongly that the ZnO films are degenerate. The mobility values are higher for the film deposited on the Si substrate compared to the glass, which may indicate a better crystal growth on Si. The doping concentration of the ZnO films are 4-5 orders of magnitude higher than that of the Si wafers used, and the ZnO/Si junction can be approximated as a metal-semiconductor junction with a depletion region occurring mainly in the Si substrate.

In fig. 2(a), a low magnification cross sectional TEM image is shown, providing the morphology of the ZnO film. The film has a thickness of ∼200 nm and displays a columnar structure with grain sizes around 20-40 nm, consistent with other reports.[15,27,28] Fig. 2(b) is a plasmon map of SiO_2, taken at an energy of 22 eV with a window of ± 2 eV. These energy-

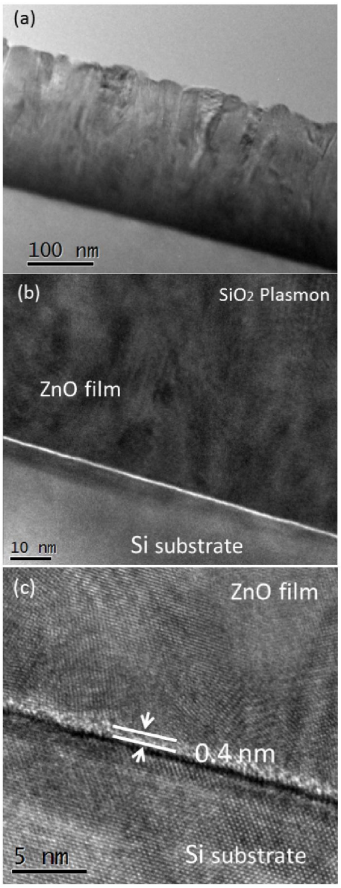

FIG. 2. Cross sectional TEM images of a ZnO/Si junction (a) low magnification image, (b) SiO_2 Plasmon map (c) high resolution image of the interface with a thin SiO_x ($x \leq 2$) layer.

filtered TEM (EFTEM) data give a qualitative information of the elemental distribution, and from the brighter contrast of the interlayer, represented as a fine white line, one can conclude that a layer of SiO_x ($x \leq 2$) exists at the interface. Indeed, Fig. 2(c) shows a high resolution micrograph of the interface, where a homogeneous SiO_x layer is observed with a thickness of less than 0.4 nm, which is substantially smaller than that of the ones previously reported in the literature.[15,22–24] Further, Fig. 2(c) unveils also that the polycrystalline growth of the ZnO grains starts at the SiO_x interface itself, as seen from their random orientation and in

agreement with previous XRD results revealing two clear reflections: (100) and (002) of the ZnO Wurtzite structure.[4]

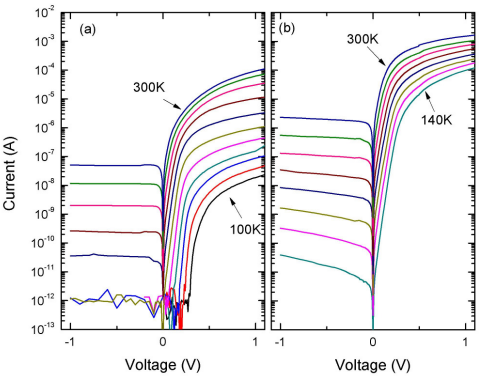

FIG. 3. (color online) Results from I-V measurements carried out at different temperature of (a) ZnO/n-Si and (b) ZnO/p-Si junctions.

Figure 3 displays results of I-V measurements performed in the 100-300K temperature range for ZnO/n-Si (a) and ZnO/p-Si (b) junctions. The data show a clear rectifying behavior for both types of substrates. At 300K, the rectification is about 3 orders of magnitude and limited by a large leakage current in the reverse direction. At lower temperatures, the reverse bias current decreases rapidly and a rectification of up to 5-6 orders of magnitude is obtained below 200K. In addition, a distinct exponential behavior of the current is observed at low forward bias voltage ($\leq$ 0.4 V) before the series resistance becomes dominant.

In analogy with a metal semiconductor junction, the Schottky-Mott model is applied to describe the I-V curves in Fig. 3. Assuming the current-transport mechanism is controlled by the thermionic-emission process,[29] the forward current is given by the relationship:

$$I/I_s = \exp(qV/nkT) - 1. \tag{1}$$

I_s is the reverse saturation current, n is the diode ideality factor, k is the Boltzmann constant and T is the absolute temperature. I_s, determined by extrapoling the straight line of ln$I$ to $V = 0$, is given by:

$$I_s = A^* A T^2 \exp(-\Phi_{bn,p}^{I-V}/kT), \tag{2}$$

where A is the contact area, A^* is the Richardson constant of Si and $\Phi_{bn,p}^{I-V}$ is the effective barrier height. The barrier heights for the ZnO/n-Si and ZnO/p-Si junctions are obtained by rearranging Eq. (2) to $\Phi_{bn,p}^{I-V} = kT\ln(A^*AT^2/I_s)$. A fit of the exponential increase of the current in the 0-0.2 V forward bias range (Fig. 3) with Eq. (1) yields $I_s(T)$ and $n(T)$.

Figure 4 depicts $\Phi_{bn,p}^{I-V}$ and n versus T for the ZnO/n-Si and ZnO/p-Si junctions. Above 280K, n is close to 1.7 but decreases then to ∼1.2 in the 280-180K temperature range. The high value above ∼280K is attributed to thermal activation of carrier generation and recombination at the ZnO/Si interface and/or in the depletion layer. Below 180K, n starts to increase again while $\Phi_{bn,p}^{I-V}$ decreases concurrently by ∼0.2 eV after being almost constant in the 300-180K range. These data suggest that the current transport below ∼180K is not only governed by thermionic-emission but also by other processes like tunneling and recombination in the interfacial/depletion region. Hence, an evaluation of the I-V data based on the thermionic-emission theory appears to be valid between ∼180K and ∼280K.

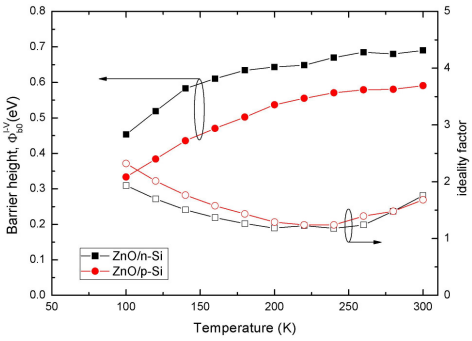

FIG. 4. (color online) Barrier height $\Phi_{bn,p}^{I-V}$ and ideality factor n versus temperature for ZnO/n-Si and ZnO/p-Si junctions.

The validity of the deduced $\Phi_{bn,p}^{I-V}$ values can also be estimated by a so-called Richardson plot. Rewriting Eq. (2) as $\ln(I_s/T^2) = \ln(A^*A) - \Phi_{bn,p}^{I-V}/kT$ and plotting $\ln(I_s/T^2)$ versus $1/kT$, $\Phi_{bn,p}^{I-V}$ can be deduced from the slope and A^* from the intercept at $1/kT = 0$. Figure 5 shows a logarithmic plot of (I_s/T^2) versus $1/kT$, where a deviation from linearity occurs for T < 200K, consistent with the decrease of $\Phi_{bn,p}^{I-V}$ in Fig. 4. Such a non-linearity is sometimes attributed to an inhomogeneous interface and variation in the barrier height.[30] However, as illustrated by Fig. 2(c), the ZnO/Si interface is smooth and not considered to cause a

significant variation in $\Phi_{bn,p}^{I-V}$. At higher temperatures, $\ln(I_s/T^2)$ is close to linear with $1/kT$ and values of $\Phi_{bn}^{I-V} = 0.61\ eV$ and $\Phi_{bp}^{I-V} = 0.52\ eV$ are obtained for the ZnO/n-Si and ZnO/p-Si junctions, respectively. Further, the sum of the two barrier heights is 1.13 eV, which is close to the band gap of Si and a self-consistent evidence of their validity. From the intercept, the values of A^* for n-type and p-type Si are extracted as ~ 6 and ~ 3 $Acm^{-2}K^{-2}$, respectively. These values are lower than the theoretical ones by about one order of magnitude[29] (112 and 32 $Acm^{-2}K^{-2}$ for n-type and p-type Si, respectively), but this can actually be regarded as a relatively small deviation compared to those found in the literature for other semiconductor materials, where discrepancies of several orders have been reported.[31,32] Furthermore, as revealed by Fig. 2, the ZnO films consist of crystalline grains with random orientation which, in addition to the thin interfacial layer of SiO_x, can slightly reduce I_s (and thus A^*).

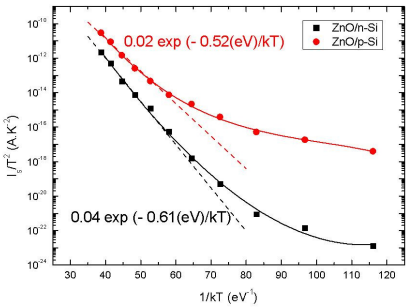

FIG. 5. (color online) The logarithm of I_s/T^2 versus $1/kT$ for ZnO/n-Si and ZnO/p-Si junction.

The barrier heights can also be estimated from the C-V measurements, $\Phi_{bn,p}^{C-V}$. In analogy with a metal-semiconductor barrier, $\Phi_{bn,p}^{C-V} = V_I + \xi + kT$ where $V_I + kT$ is the built-in voltage and ξ is the difference between the Fermi level position and the conduction/valence band edge in n-type/p-type material. The built-in voltage is related to the depletion capacitance by:

$$\frac{1}{C^2} = \frac{2}{A^2 \epsilon q N_{D,A}}(V_I + V_{rb}), \tag{3}$$

where ϵ is the permitivity of Si, $N_{D,A}$ is the majority carrier concentration in Si and V_{rb} is the applied bias voltage. Figure 6 shows $1/C^2$ versus V_{rb} at different temperatures

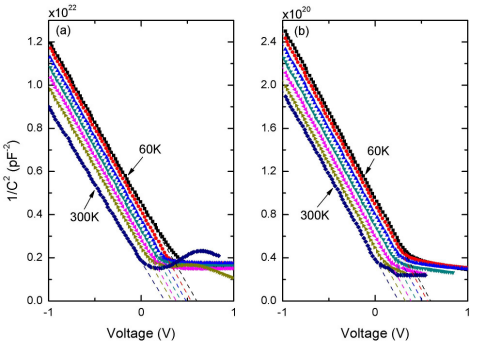

FIG. 6. $1/C^2$ versus bias voltage of (a) ZnO/n-Si and (b) ZnO/p-Si junctions at different sample temperatures between 60 and 300K.

TABLE I. Average values of barrier heights and ZnO work function obtained from I-V (Richardson plots) and C-V measurements in the temperature range 60-300K, for ZnO/n-Si and ZnO/p-Si junctions.

	Φ_b^{IV} (eV)	Φ_{ZnO}^{IV} (eV)	Φ_b^{CV} (eV)	Φ_{ZnO}^{CV} (eV)
ZnO/n-Si	0.61	4.66	0.66	4.71
ZnO/p-Si	0.52	4.65	0.58	4.59

for ZnO/n-Si and ZnO/p-Si junctions. A linear relation holds accurately in the reverse bias range and the built-in voltage is estimated from the intercept of $1/C^2$ with the abscissa. The $\Phi_{bn,p}^{C-V}$ values deduced are constant with $\pm$ 0.02 eV in the 60-300K temperature range and the average ones are given in Table I; they are slightly higher than those from the I-V data, possibly associated with image force lowering in the latter case despite the fact that the sum of Φ_{bn}^{IV} and Φ_{bp}^{IV} is very close to E_g. Based on the Φ_b values and omitting the influence of the minute SiO_x interfacial layer, Φ_{ZnO} can be estimated using the electron affinity of Si (χ_{Si}), $\Phi_{ZnO} = \Phi_{bn} + \chi_{Si}$ and $\Phi_{ZnO} = E_g(T) + \chi_{Si} - \Phi_{bp}$ for the ZnO/n-Si and ZnO/p-Si junctions, respectively. Table I summarizes the results and within an accuracy of ≤ 0.10 eV, Φ_{ZnO} is equal to 4.65 eV.

IV. CONCLUSIONS

Highly n-doped films of ZnO have been grown on n- and p-type Si substrates by ALD. The films display a columnar structure with randomly oriented grains and an excellent interface to the Si substrates with a very thin ($\leq$ 0.4 nm) intermediate layer of SiO_x. Both the ZnO/n-Si and ZnO/p-Si heterojunctions exhibit strong rectifying behavior, and above $\sim$180K, the current transport is dominated by thermionic emission. Self consistent values of Φ_{bn} and Φ_{bp} are deduced from both I-V-T and C-V-T data and accordingly, Φ_{ZnO} is found to be 4.65 eV with an accuracy better than $\pm$0.10 eV.

ACKNOWLEDGMENTS

This work was financially supported by the Norwegian Research Council through the NanoMat (CONE project) and FRIENERGI programs.

REFERENCES

[1]C.W. Litton, D.C. Reynolds, and T.C. Collins. *Zinc Oxide Materials for Electronic and Optoelectronic Device Applications*. Wiley, 2011.

[2]A. Yamada, B. Sang, and M. Konagai. *Appl. Surf. Sci.*, 112:216, 1997.

[3]S.J. Lim, S. Kwon, and H. Kim. *Thin solid films*, 516:1523, 2008.

[4]V. Quemener, M. Alnes, L. Vines, O. Nilsen, H. Fjellvåg, E.V. Monakhov, and B.G. Svensson. *Solid State Phenomena*, 178:130, 2011.

[5]K. Schulze, B. Maennig, K. Leo, Y. Tomita, C. May, J. Hüpkes, E. Brier, E. Reinold, and P. Bäuerle. *Appl. Phys. Lett.*, 91:073521, 2007.

[6]W. Li, C.W. Wu, W.G. Qin, G.C. Wang, S.Q. Lu, X.J. Dong, H.B. Dong, and Q.L.Sun. *Physica B*, 404:2197, 2009.

[7]J.-H. Park, K.-J. Ahn, K.-I. Park, S.-I. Na, and H.-K. Kim. *J. Phys. D: Appl. Phys.*, 43:115101, 2010.

[8]R. Jaramillo and S. Ramanathan. *Sol. Energ. Mat. Sol. C.*, 95:602, 2011.

[9]X. Jiang, F.L. Wong, M.K. Fung, and S.T. Lee. *Appl. Phys. Lett.*, 83:1875, 2003.

[10]T.W. Kim, D.C. Choo, Y.S. No, W.K. Choi, and E.H. Choi. *Appl. Surf. Sci.*, 253:1917, 2006.

[11]A. Klein, C. Körber, A. Wachau, F. Säuberlich, Y. Gassenbauer, R. Schafranek, S.P. Harvey, and T.O. Mason. *Thin Solid Films*, 518:1197, 2009.

[12]G. B. Murdoch, S. Hinds, E. H. Sargent, S. W. Tsang, L. Mordoukhovski, and Z. H. Lu. *Appl. Phys. Lett*, 94:213301, 2009.

[13]T.L. Tansley and S.J.T. Owen. *J. Appl. Phys.*, 55:454, 1984.

[14]K. B. Sundaram and A. Khan. *J. Vac. Sci. Technol. A*, 15:428, 1997.

[15]D. Song, D.-H. Neuhaus, J. Xia, and A. G. Aberle. *Thin Solid Films*, 422:180, 2002.

[16]D. Song, B. Guo, and A.G. Aberle. In *Conference on Optoelectronic and Microelectronic Materials and Devices*, 2002.

[17]H.H. Afify, S.H. EL-Hefnawi, A.Y. Eliwa, M.M. Abdel-Naby, and N.M. Ahmed. *Egypt. J. Solids*, 28:243, 2005.

[18]Ş . Aydoğan, K. Çınar, H. Asıl, C. Coşkun, and A. Türüt. *Journal of Alloys and Compounds*, 476:913, 2009.

[19]N. Zebbar, M.S. Aida, A.E.K. Hafdallah, O. Daranfad, H. Lekiket, and M. Kechouane. *Mater. Sci. Forum*, 609:133, 2009.

[20]V. Quemener, L. Vines, E.V. Monakhov, and B.G. Svensson. *Thin solid films*, 519:5763, 2011.

[21]H. Malmbekk, L. Vines, E.V. Monakhov, and B.G. Svensson. *J. Appl. Phys.*, 110:074503, 2011.

[22]W.G. Han, S.G. Kang, T.W. Kim, D.W. Kim, and W.J. Cho. *Appl. S*, 245:384, 2005.

[23]T.H. Breivik, S. Diplas, A.G. Ulyashin, A.E. Gunnæs, B.R. Olaisen, D.N. Wright, A. Holt, and A. Olsen. *Thi*, 515:8479, 2007.

[24]Y. Choi, K. Lee, C.H. Park, K.H. Lee, J.-W. Nam, M.M. Sung, K.M. Lee, H.C. Sohn, and S. Im. *J. Phys. D: Appl. Phys.*, 43:115101, 2010.

[25]N. Huby, S. Ferrari, E. Guziewicz, M. Godlewski, , and V. Osinniy. *Appl. Phys. Lett*, 92:023502, 2008.

[26]T. Krajewski, E. Guziewicz, L. Wachnicki, I.A. Kowalik, A. Wojcik-Glodowska, M. Lukasiewicz, K. Kopalko, V. Osinniy, and M. Guziewicz. *Microelectronics Journal*, 40:293–295, 2009.

[27]K. T. Roro, G. H. Kassier, J. K. Dangbegnon, S. Sivaraya, J. E. Westraadt, J H Neethling, A. W. R. Leitch, and J. R. Botha. *Semicond. Sci. Technol.*, 23:055021, 2008.

[28]C. Major, A. Nemeth, G. Radnoczi, Zs. Czigany, M. Fried, Z. Labadi, and I. Barsony. *Applied Surface Science*, 255:8907, 2009.

[29]E.H. Rhoderick and R.H. Williams. *Metal-Semiconductor contacts.* Oxford university press, 1988.

[30]J. H. Werner and H. H. Güttler. *J. Appl. Phys.*, 69:1522, 1991.

[31]A. Tataroğlu and Ş Altındal. *J. Alloy and Compd*, 479:893, 2009.

[32]W. Mtangi, F.D. Auret, C. Nyamhere, P.J. Janse van Rensburg, M. Diale, and A. Chawanda. *Physica B*, 404:1092, 2009.